CHAPTER IV
RESULTS AND DISCUSSION

4.1 Characterization of Synthesized PBA

4.1.1 Molecular Weight Variation

The molecular weight of PBA was varied by changing the types of solvent and metal halide; the amount of solvent; the reaction time; and the amount of phosphorus compound. The experimental conditions are tabulated in Table 4.1.

4.4.1.1 *The effect of type of solvent and metal halide*

The reaction was assumed to proceed as followed: triphenyl phosphite (TPP) reacted with metal halide to produce a phosphonium salt (I), which then reacted with carboxylic acid to give acyloxyphosphonium salt (II). Acyloxyphosphonium salt (II) then reacted with amine as shown in Scheme 2. Among the metal halides examined, the additions of LiCl and $CaCl_2$ show favorable effects upon the yield and the molecular weight of polymer. LiCl is the most effective amongst the two (Hagashi *et al.*, 1980); because lithium ion is the smallest monocation so it yields the most stability metal complex (I). The amide solvent effects can not be explained by solubility alone. It is assumed that solvents may have some effect upon the formation and the reactivity of I and II as presented in the Scheme 2. DMAc and NMP are effective among tested solvents. NMP is the most favorable solvent (Hagashi *et al.*, 1980) due to it's higher solubility parameter [23.1 $(MPa)^{1/2}$] than DMAc [22.1 $(MPa)^{1/2}$] (Brandrup and Immergut, 1989). For the systems number 1 and 2 in Table 4.1, changing the solvent from DMAc to NMP and metal halide from $CaCl_2$ to LiCl dramatically increase the molecular weight.

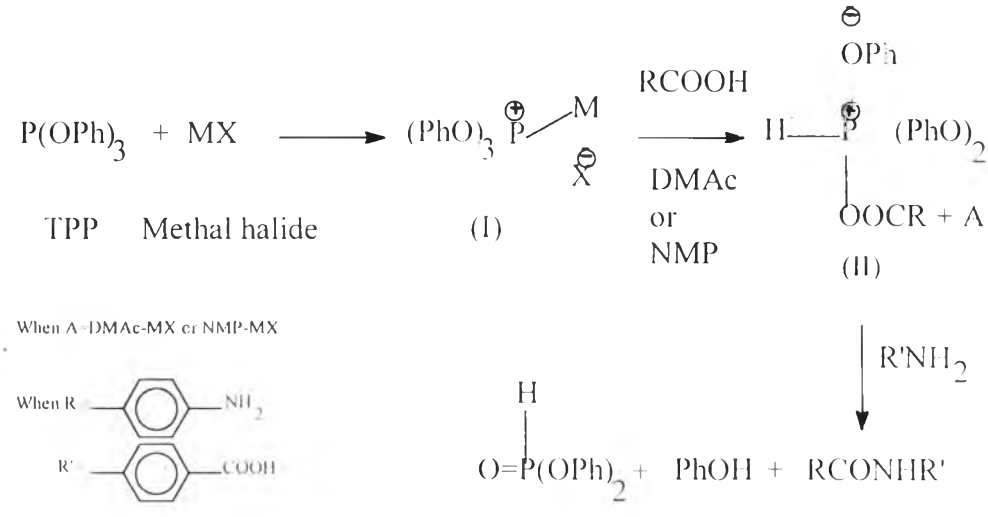

Scheme 2.

4.1.1.2The effect of amount of solvent

The amount of the solvent used is sufficient for placing the starting materials used in the present process in a homogeneous liquid phase. Usually, the solvent is preferably used in a condition that concentration of the monomer is in a range between 0.2 to 2.0 moles per liter of the solvent (Yamazaki and Higashi, 1975). For the systems in Table 4.1, the monomer concentrations used of the monomer were in a suitable range so changing the amount of solvent does not affect the molecular weight. PBA-2's concentration was in the middle of the range so the reaction yielded the highest M_w polymer.

4.4.1.3*The effect of reaction time*

The relationship between molecular weight (MW), degree of polymerization (X_n), and reaction time (t) of condensation polymerization is shown in Figure 4.1 (Painter and Colemar, 1994). At the beginning, X_n very slowly increases because each monomer polymerizes to obtain many short chains. At a suitable time (t_s), every short chain polymerizes to give long chains so x_n rapidly increases with time.

Higashi *et al.*, reported that reaction time of 2 h was long enough and there has been no further improvement in the viscosity of polymer solution produced after an additional 2 h (Hagashi *et al.*, 1980). For the systems number 5 and 6 in Table 4.1, the suitable reaction time of these reactions is 2 h so changing the reaction time does not affect the molecular weight.

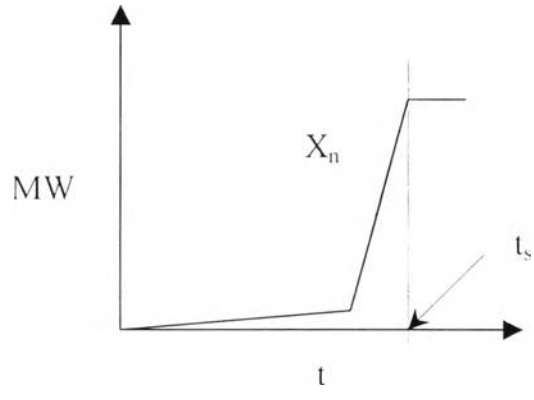

Figure 4.1 The relationship between molecular weight (MW), degree of polymerization (X_n), and reaction time (t) of condensation polymerization when X_n is equal to number average molecular weight (M_n) over molecular weight of repeating unit.

4.1.1.4*The effect of amount of phosphorus compound*

Several phosphorus compounds were examined in the polycondensation of *p*-ABA in the present of LiCl. Triphenyl phosptite (TPP) is the most effective. An equivalent of the phosphite to *p*-ABA give polymer of the highest solution viscosity, but further addition decreased the viscosity of the resulting polymer solution (Hagashi *et al.*, 1980).

Higashi *et al.*, have shown that triphenyl phosphite can activate in an equivalent to carboxylic acids in the present of pyridine via acyloxy N-phyphonium salt (III) similar to II as shown in Scheme 3. For the systems number 6 and 7 in Table 4.1, an increase in the amount of phosphorus compound slightly decreases the molecular weight.

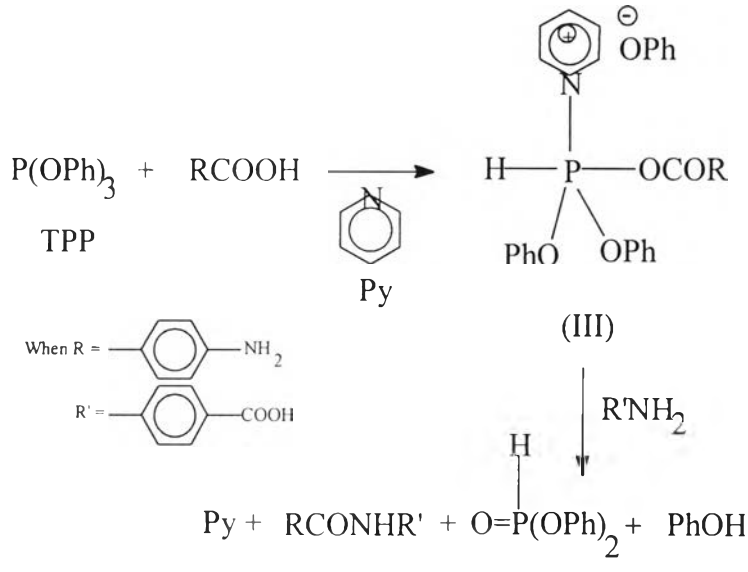

Scheme 3.

Table 4.1 Summary of molecular weight variation of PBA

System	Solvent	Metal Halide	Mole *p*-ABA : TPP : Solvent	C of *p*-ABA to solvent (mol/l)	Time (h)	[b]M_w (g/mol)	Name
1	DMAc	$CaCl_2$	1 : 1 : 10	1	2	3,900	PBA-1
2	NMP	LiCl	1 : 1 : 10	1	2	11,000	PBA-2
3	NMP	LiCl	1 : 1 : 20	0.5	2	10,000	PBA-3
4	NMP	LiCl	1 : 1 : 30	0.35	2	10,000	PBA-4
5	NMP	LiCl	1 : 1 : 20	0.5	2	10,000	PBA-5
				0.5	4	10,000	PBA-6
				0.5	6	10,000	PBA-7
				0.5	8	10,000	PBA-8
6	NMP	LiCl	1 : 2 : 20	0.5	2	8,600	PBA-9
				0.5	4	8,700	PBA-10
7	NMP	LiCl	1 : 2 : 30	0.35	2	8,700	PBA-11

[b]M_w of PBA were determined by viscometry at 25°C in 96% H_2SO_4. The raw data are tabulated in Appendix B.

Condensation polymerization requires the reaction between different function groups from different polymer chains (Painter and Colemar, 1994). PBA contains aromatic rings in its backbone which provides a high rigidity to the main chains. With such high rigidity, the chains tend to take up an extended chain conformation. The molecules are para-substituted giving a structure of high regularity and planarity. This enables the molecules to get close together for maximum intermolecular interactions and maximum packing. There are extensive H-bondings between adjacent molecules. The molecules behave like rigid-rod (rodlike) (Rivas *et al.*, 1996 and Kroschmiz and Marry, 1995). Their molecules were very difficult to move or to react with each another as the reaction time reached 2 h. That is why the yield of the highest M_w polymer obtained was low.

To solve this problem, dilutions of system 2 were attempted. After 2 h of the reaction time, the reaction mixture was diluted four and eight times by NMP, then further polymerized 2 h at 100 ^{0}C. The results are tabulated in Table 4.2.

Table 4.2 Molecular weight of PBA in dilute systems

System	Dilution (Times)	Concentration of *p*-ABA to solvent (mol/l)	[b]M_w (g/mol)	Name
8	4	0.2	10,000	PBA-12
9	8	0.1	10,000	PBA-13

From Table 4.2, the molecular weights of both systems do not increase. Because the concentrations of the monomer to solvent were below the suitable range (0.2-2 moles per liter) so the polymer chains were too far to react with one another to produce longer chains.

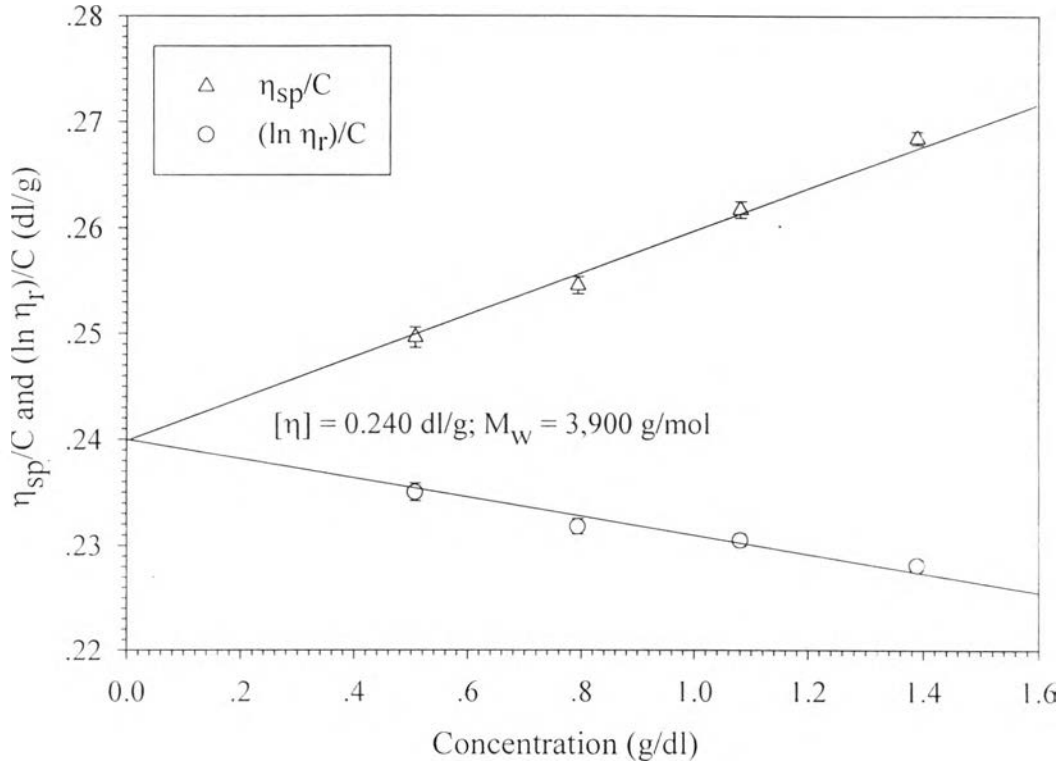

Figure 4.2 η_{sp}/C and (ln η_r)/C versus PBA concentration of PBA-1 at 25^0C.

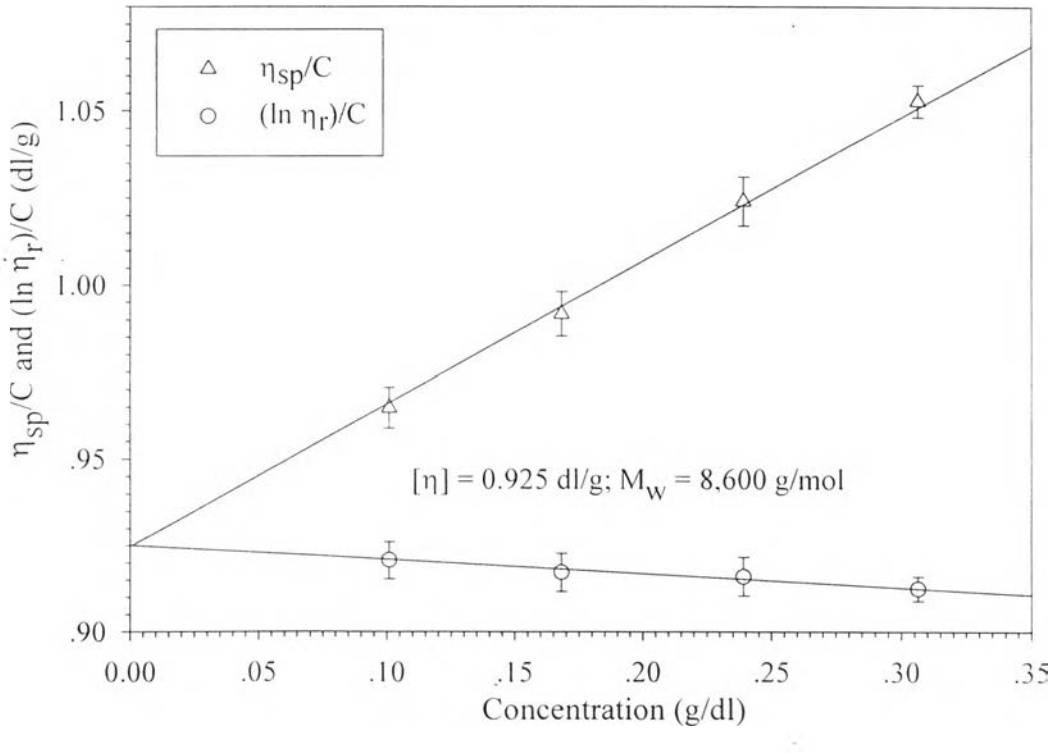

Figure 4.3 η_{sp}/C and (ln η_r)/C versus PBA concentration of PBA-9 at 25^0C.

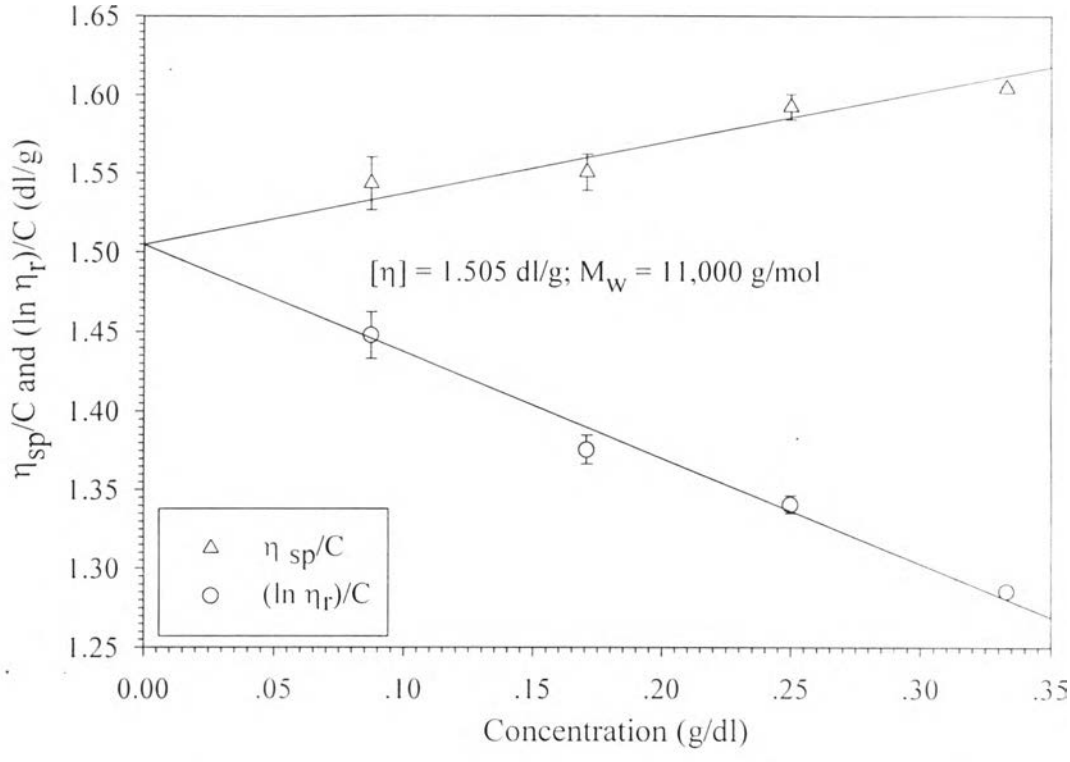

Figure 4.4 η_{sp}/C and (ln η_r)/C versus PBA concentration of PBA-2 at 25^0C.

In summary, the three different materials obtained, designated PBA-1; PBA-9 and PBA-2, have M_w = 3,900; 8,600 and 11,000 g/mol, respectively. Their plots between the reduced viscosity, η_{sp}/C and the inherent viscosity, (ln η_r)/C versus PBA concentration (C) in 96% H_2SO_4 at 25^0C are shown in Figures 4.2, 4.3, and 4.4; respectively. They were further characterized by FTIR, UV-VIS, ^{13}C-NMR, DSC and TGA.

4.1.2 Spectroscopic Characterization

4.1.2.1 *Fourier Transform Infrared Spectroscopy (FTIR)*

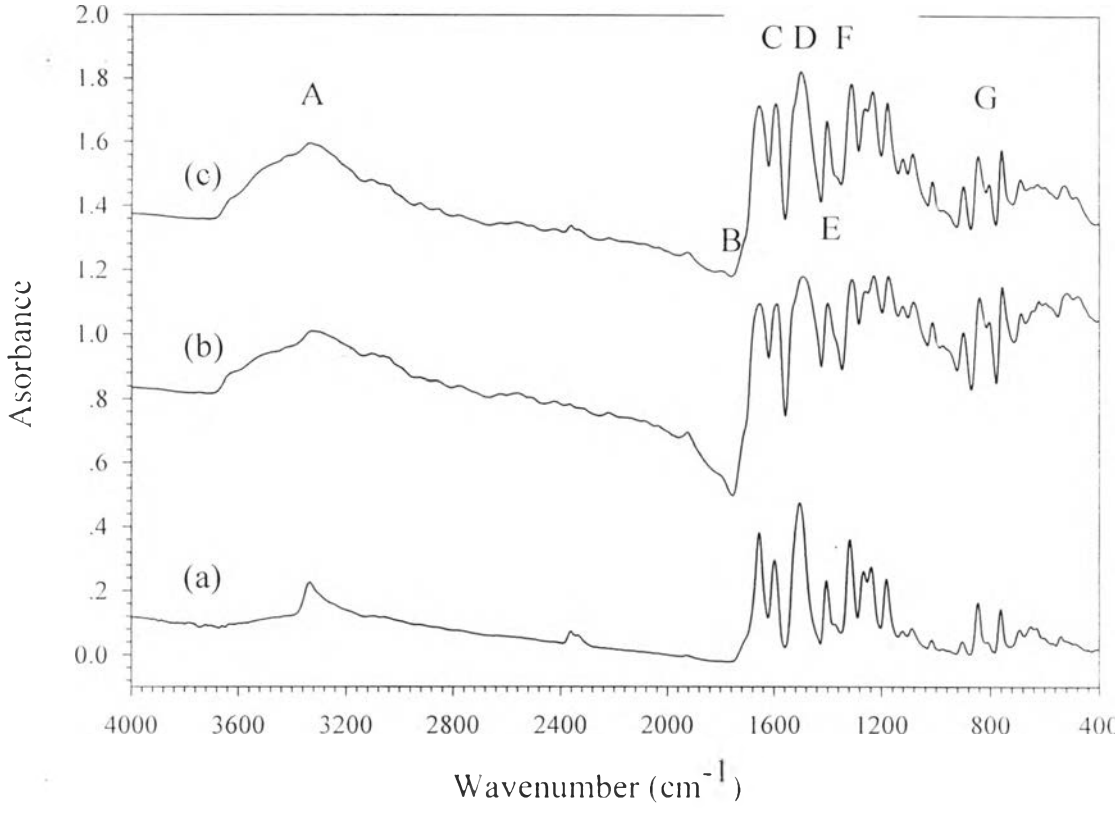

Figure 4.5 The FTIR spectra of PBA: (a) PBA-1, (b) PBA-2, and (c) PBA-9.

FTIR Spectra of PBA are shown in Figure 4.5. All PBA show similar FTIR spectra. The main absorption peaks are tabulated in Table 4.3. The absorption peaks at 3335, 1655, 1505, and 1317 cm^{-1} indicate the characteristic peaks of amide. The absorption peaks at 1598 and 846 cm^{-1} indicate the characteristic peaks of the benzene ring and the para substituted on the benzene ring, respectively (Rivas *et al.*, 1996 and Campbell and White, 1989).

4.1.2.2*Ultraviolet-Visible Spectroscopy (UV-VIS)*

UV-VIS spectra of PBA are shown in Figures 4.6 and 4.7.

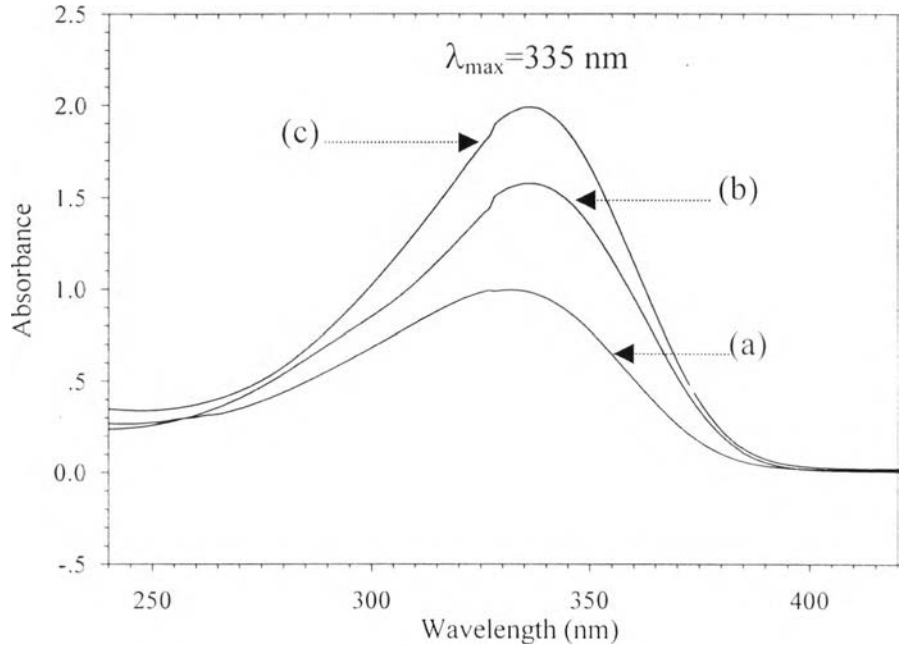

Figure 4.6 The UV-VIS spectra of PBA in 96% H_2SO_4: (a) PBA-1 (10 ppm), (b) PBA-2 (15 ppm), and (c) PBA-9 (18 ppm).

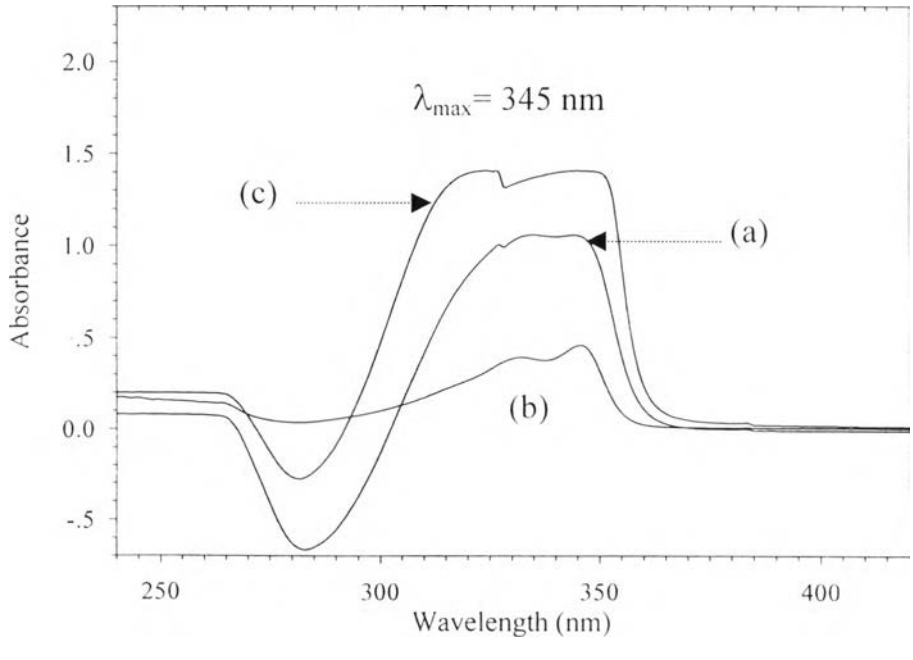

Figure 4.7 The UV-VIS spectra of PBA in 3% LiCl/DMAc: (a) PBA-1 (16 ppm), (b) PBA-2 (10 ppm), and (c) PBA-9 (18 ppm).

All PBA show similar UV-VIS spectra. The spectra of PBA in 96% H_2SO_2 and 3%LiCl in DMAc show a maximum absorption peak (λ_{max}) at wavelengths around 335 and 345 nm. respectively. These bands are defined as $n \rightarrow \pi^*$ transition of carbonyl (C=O) group due to shifting of λ_{max} to s higher value for the lower polar solvent. In addition, the spectra of PBA in 96% H_2SO_2 are broader than in 3% LiCl/DMAc because a polar solvent tends to eliminate the fine peaks arising from different vibrational states (Conio *et al.*, 1998).

Table 4.3 Remarks and assignments of peaks from FTIR spectra for PBA (Campbell and White, 1989)

	Wavenumber (cm^{-1})	Remarks and Assignments
A	3335	N-H stretching of secondary amide
B	1655	C=O stretching of amide
C	1598	C=C stretching of aromatic ring Carboxylate asymmetric stretching
D	1505	N-H bending of secondary amide
E	1404	Carboxylate symmetric stretching
F	1317	C-N stretching of aromatic amide
G	846	=C-H bending of para substitution on aromatic ring

4.2.1.3 *^{13}C-Neuclear Magnetic Resonance (^{13}C-NMR)*

^{13}C-NMR spectrum of PBA-1 in solution state is shown in Figure 4.8. The main absorption peaks are tabulated in Table 4.4.

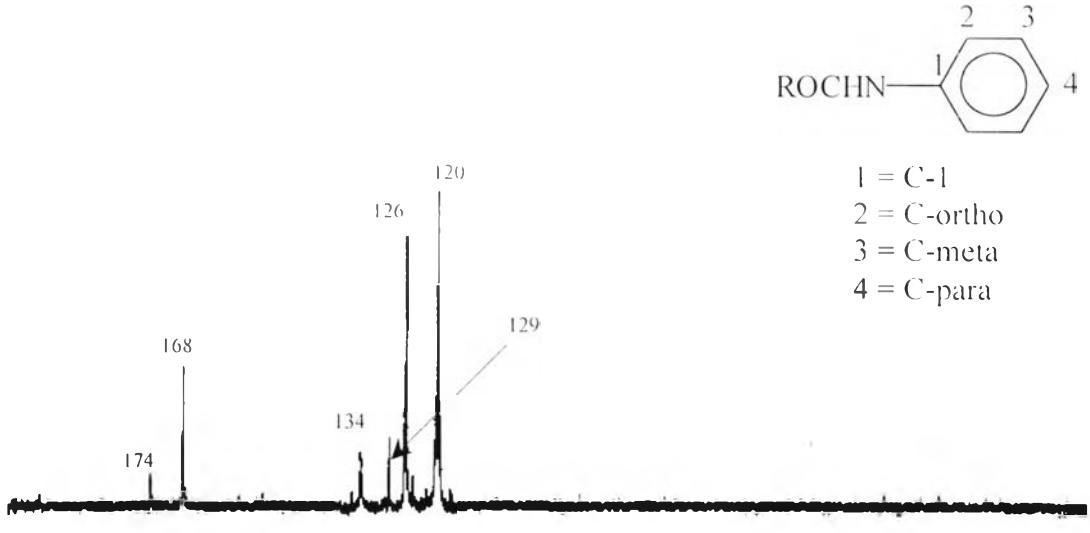

Figure 4.8 The solution state ^{13}C-NMR spectrum of PBA-1 in 98 % D_2SO_4.

Table 4.4 Remarks and assignments of peaks from the solution state ^{13}C-NMR spectrum for PBA-1 (Campbell and White, 1989)

Chemical Shift (ppm)	Remarks and Assignments
174	C of carboxylic acid at the end chain
168	C of C=O in repeating unit
134	C of C-1 on benzene ring
129	C of C-meta on benzene ring
126	C of C-para on benzene ring
120	C of C-ortho on benzene ring

The absorption peaks at 174 and 168 ppm indicate the characteristic peaks of carbon of carbonyl (C=O) group. The absorption peaks at 134, 129, 126 and 120 ppm indicate the characteristic peaks of carbon of the substituted on benzene ring. ^{13}C CP/MAS NMR spectrum of PBA-1, PBA-2 and PBA-9 in solid state are shown in Figure 4.9, 4.10 and 4.11, respectively.

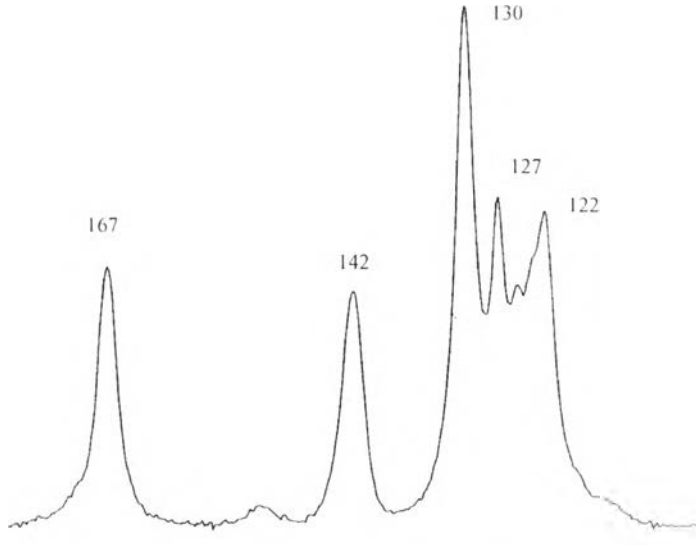

Figure 4.9 The solid state ^{13}C CP/MAS NMR spectrum of PBA-1.

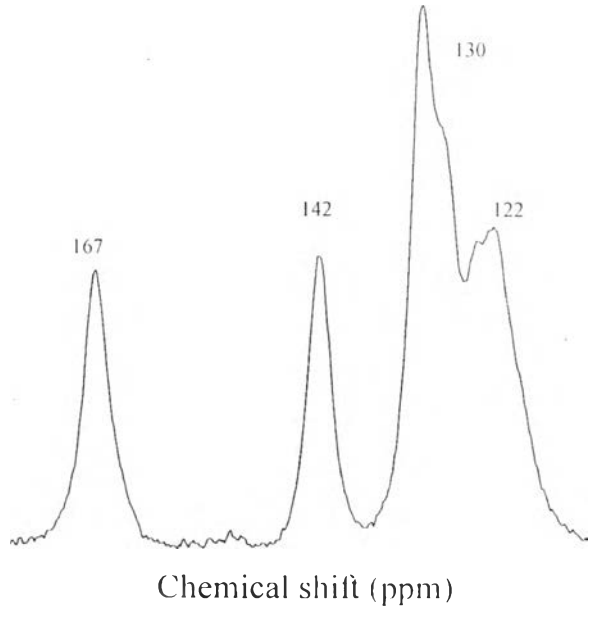

Figure 4.10 The solid state ^{13}C CP/MAS NMR spectrum of PBA-2.

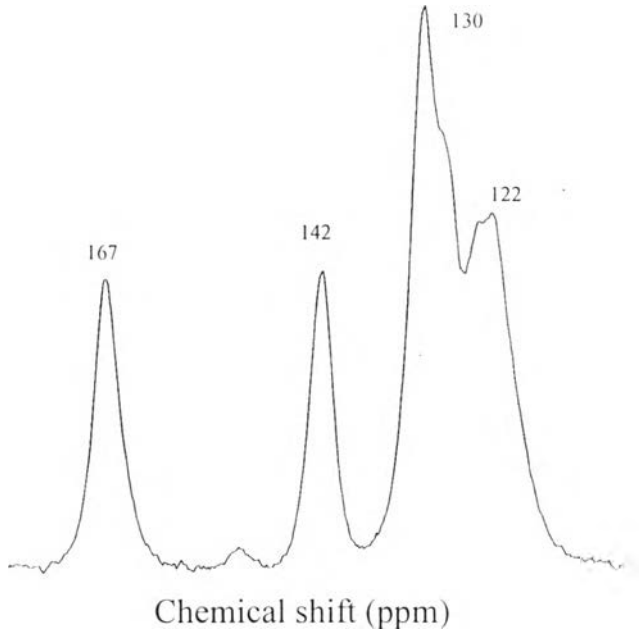

Figure 4.11 The solid state ^{13}C CP/MAS NMR spectrum of PBA-9.

Magnetic dipoles of carbon atoms in solid state are fixed. They are coupled to one another. This phenomenon is called dipolar coupling (Campbell and White, 1989). So ^{13}C NMR spectra in solid state (Figures 4.9, 4.10 and 4.11)show broad peaks when comparing with ^{13}C NMR spectrum in solution state (Figure 4.8). However, all ^{13}C NMR spectra in solid state show the specific peaks of carbonyl group (167 ppm) and benzene ring (122-142 ppm) like ^{13}C NMR spectrum in solution state. The higher the molecular weight, the higher dipolar coupling, the broader peaks are obtained. PBA-2 and PBA-9 having higher molecular weights, peaks at 130 and 127 ppm are overlaped to each other unlike PBA-1. Because, PBA-2 and PBA-9 are slightly different in molecular weight so they have similar spectra.

From spectroscopic characterization and molecular weight determination, PBA were successfully synthesized to yield different molecular weights by changing the types of solvent and metal halide, and the amount of the phosphorus compound used.

4.1.3 Thermal Analysis

4.1.3.1 *Differential Scanning Calorimetry (DSC)*

The DSC thermograms of PBA are shown in Figure 4.12.

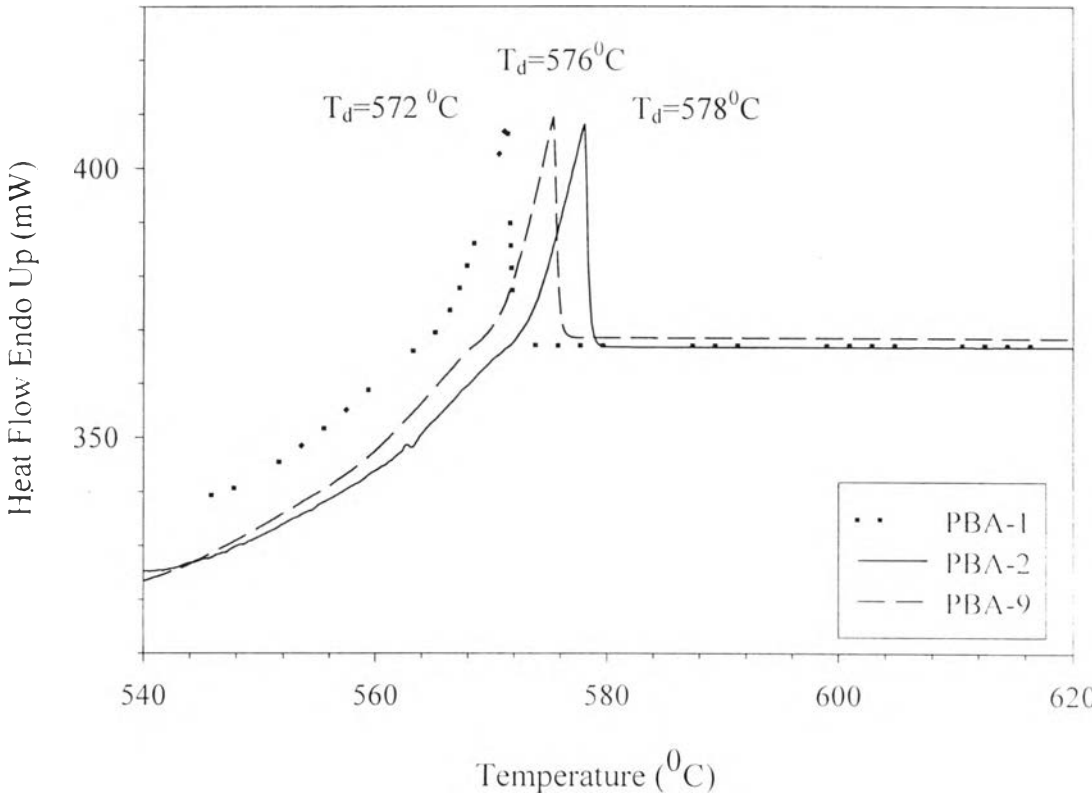

Figure 4.12 The DSC thermograms of PBA.

All PBA show similar DSC thermograms. There are endothermic peaks at around 575°C referring to the decomposition temperature (T_d) of PBA (Takase *et al.*, 1986). In addition, T_d increases slightly with molecular weight.

4.3.1.2 *Thermogravimetric Analyzer (TGA)*

The TGA thermograms of PBA are shown in Figure 4.13.

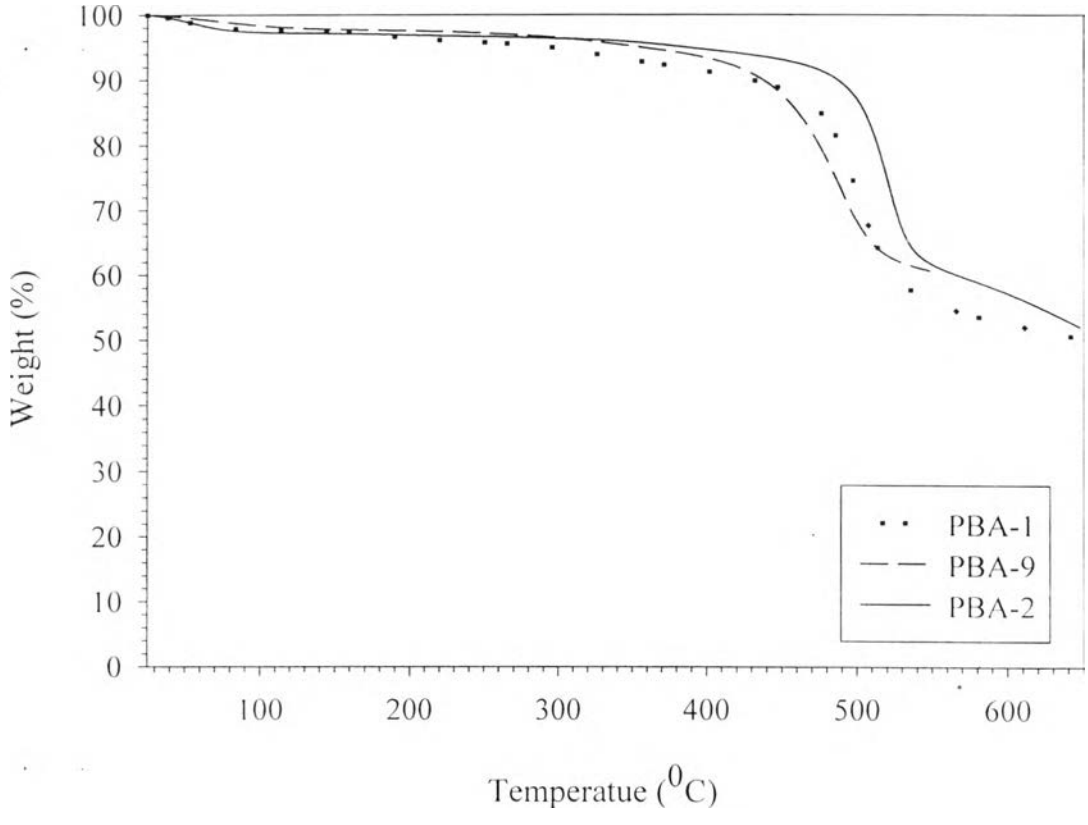

Figure 4.13 The TGA thermograms of PBA.

All PBA show similar TGA thermograms. They are thermally stable up to around 500°C. Beyond that temperature, their masses are lost rapidly due to breaking of their main chains (Takase *et al.*, 1986). Higher molecular weight PBA has higher thermal stability. These results agree well with the present DSC results. In conclusion for the thermal analysis, synthesized PBA are thermally stable.

4.2 The formation of Liquid Crystalline Phase of PBA Solution

The formation of liquid crystalline (LC) phase of PBA solution was determined by measuring the zero-shear rate solution viscosity, η_o, (P, poise) versus PBA concentration (wt%) (the raw data are tabulated in Appendix C) and visual observations through an optical polarizing microscope with crossed polars.

The formation of LC phase of polyamides can be affected by the polymer structure, the molecular weight, the polymer-solvent interaction and temperature (Mark *et al.*, 1987). PBA-1 and PBA-2 were studied for the effect of molecular weight. 4%LiCl/DMAc and 4%LiCl/NMP were studied for the effect of polymer-solvent interactions. To avoid the effect of temperature, the experiment was carried out at 25 ± 1^0C.

4.2.1 The Effect of Polymer Structure

From Figure 1.4, PBA contains benzene rings in its backbone which provide high rigidity to the main chains (rod-like structure). The molecules are para-substituted which have the extended chain conformation to facilitate the alignment of the polymer chain along a particular direction. In addition, there are extensive H-bondings between adjacent molecules (Mark *et al.*, 1987). So PBA can form LC phase in solution at a certain concentration and temperature.

4.2.1.1 *Viscosity Measurement*

Figures 4.14, 4.15, 4.16 and 4.17 show the zero-shear rate viscosity at 25^0C as a function of the PBA-2 concentration in 4%LiCl/DMAc, the PBA-2 concentration in 4%LiCl/NMP, the PBA-1 concentration in

4%LiCl/DMAc and the PBA-1 concentration in 4%LiCl/NMP, respectively. Possible mechanism of the four regimes are proposed (Scheme 4):

Regime I, for the effect of concentration, the viscosity slightly increases with PBA concentration in the normal way like an isotropic phase (Nakasima, 1994). This phenomenon was confirmed by optical textures as shown in Figures 4.20 (a), 4.21 (a), 4.22 (a) and 4.23 (a) for PBA-2 in 4%LiCl/DMAc, PBA-2 in 4%LiCl/NMP, PBA-1 in 4%LiCl/DMAc and PBA-1 in 4%LiCl/NMP, respectively.

Regime II, the viscosity rises dramatically up to the maximum viscosity due to the effect of phase change. However, LC phases start to form due to the effect of PBA structure. The smaller the movement of the polymer chain, the higher the viscosity, and the easier the LC phase is formed. So the isotropic-anisotropic transition is located before the maximum of the curve (Salamone, 1996). It is biphasic phase where a LC phase coexists with an isotropic phase. This phenomenon is confirmed by optical textures as shown in Figures 4.20 (b), 4.21 (b), 4.22 (b) and 4.23 (b) for PBA-2 in 4%LiCl/DMAc, PBA-2 in 4%LiCl/NMP, PBA-1 in 4%LiCl/DMAc and PBA-1 in 4%LiCl/NMP, respectively.

Region III, for the effect of PBA structure, when PBA molecules are so crowded they restrict the movement of one another, LC phases are formed more and more leading to a reduction in the occupied volume and hence the viscosity starts to decrease (Nakajima, 1994). It is biphasic phase where an isotropic phase coexists with a LC phase. This phenomenon is confirmed by optical textures as shown in Figures 4.20 (c), 4.21 (c), 4.22 (c) and 4.23 (c) for PBA-2 in 4%LiCl/DMAc, PBA-2 in 4%LiCl/NMP, PBA-1 in 4%LiCl/DMAc and PBA-1 in 4%LiCl/NMP, respectively. As concentration increases, the viscosity reaches a minimum.

Region IV, for the effect of concentration, when the number of polymer molecules further increases, they can no longer be compensated by reduction in the occupied volume and hence viscosity starts to increase again (Nakajima, 1994). It is a fully LC phase. This phenomenon is confirmed by optical textures as shown in Figures 4.20 (d), 4.21 (d), 4.22 (d) and 4.23 (d) for PBA-2 in 4%LiCl/DMAc, PBA-2 in 4%LiCl/NMP, PBA-1 in 4%LiCl/DMAc and PBA-1 in 4%LiCl/NMP, respectively.

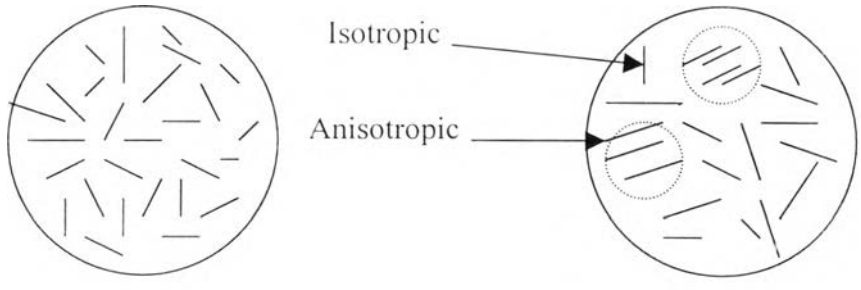

I : Isotropic Phase

II : Biphasic Phase

(Isotropic phase in anisotropic phase)

III : Biphasic Phase

IV : Fully LC Phase

(Anisotropic phase in isotropic phase)

Scheme 4.

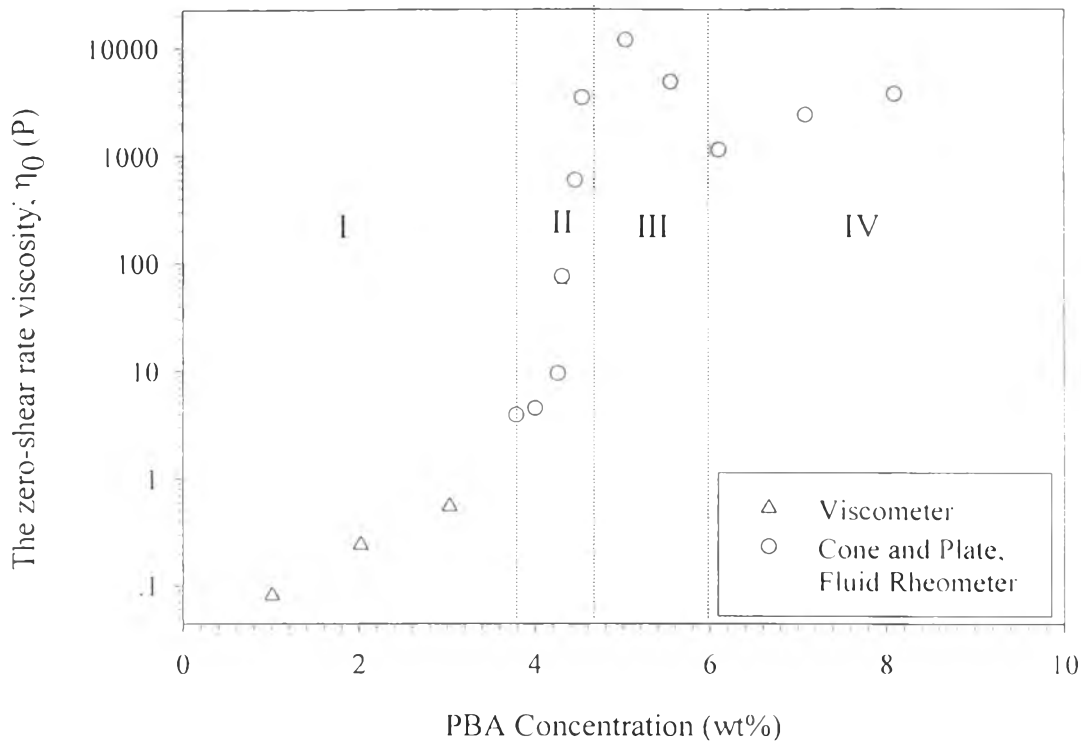

Figure 4.14 The zero-shear rate viscosity of PBA-2 in 4%LiCl/DMAc at 25^0C.

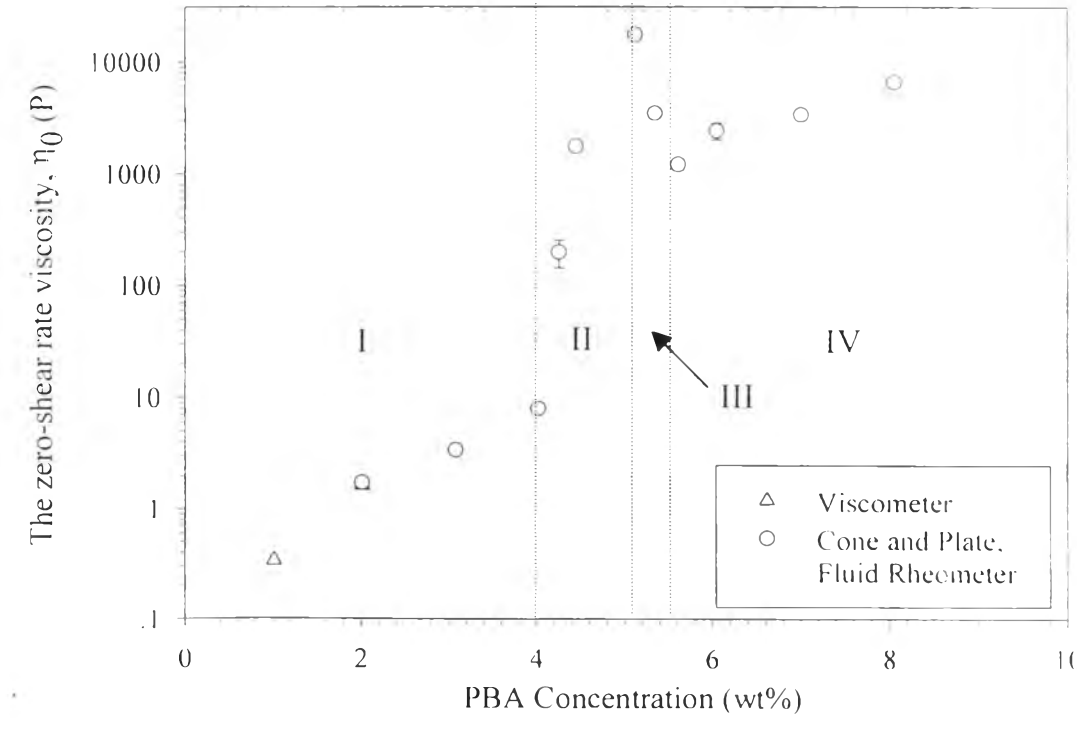

Figure 4.15 The zero-shear rate viscosity of PBA-2 in 4%LiCl/NMP at 25^0C.

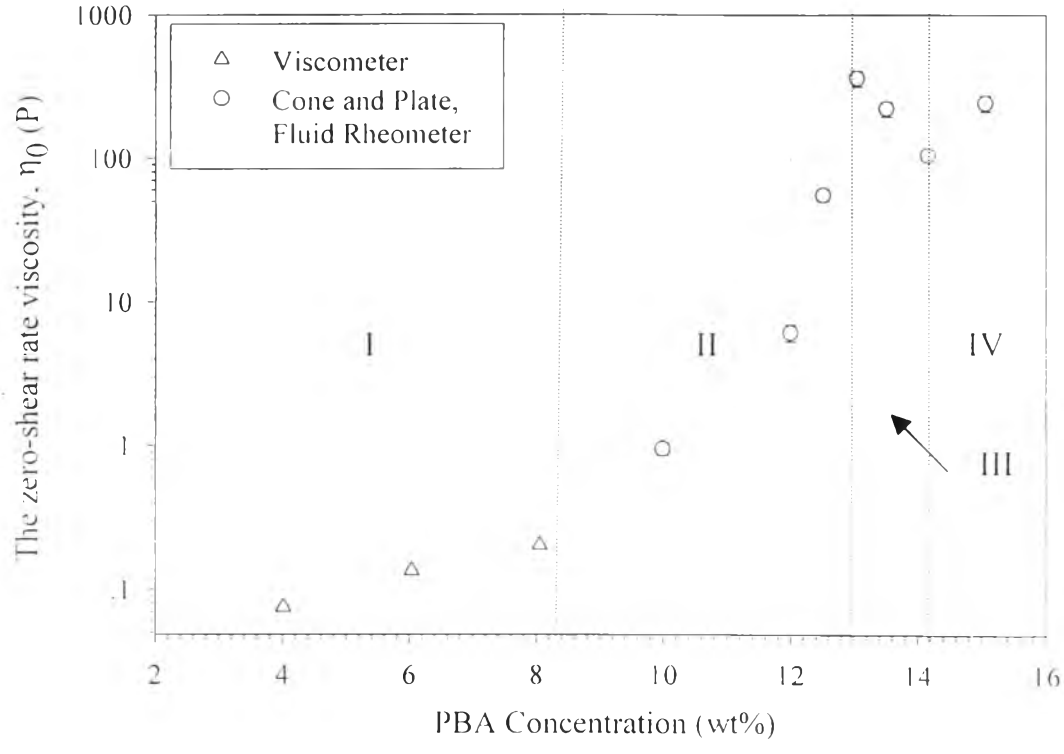

Figure 4.16 The zero-shear rate viscosity of PBA-1 in 4%LiCl/DMAc at 25^0C.

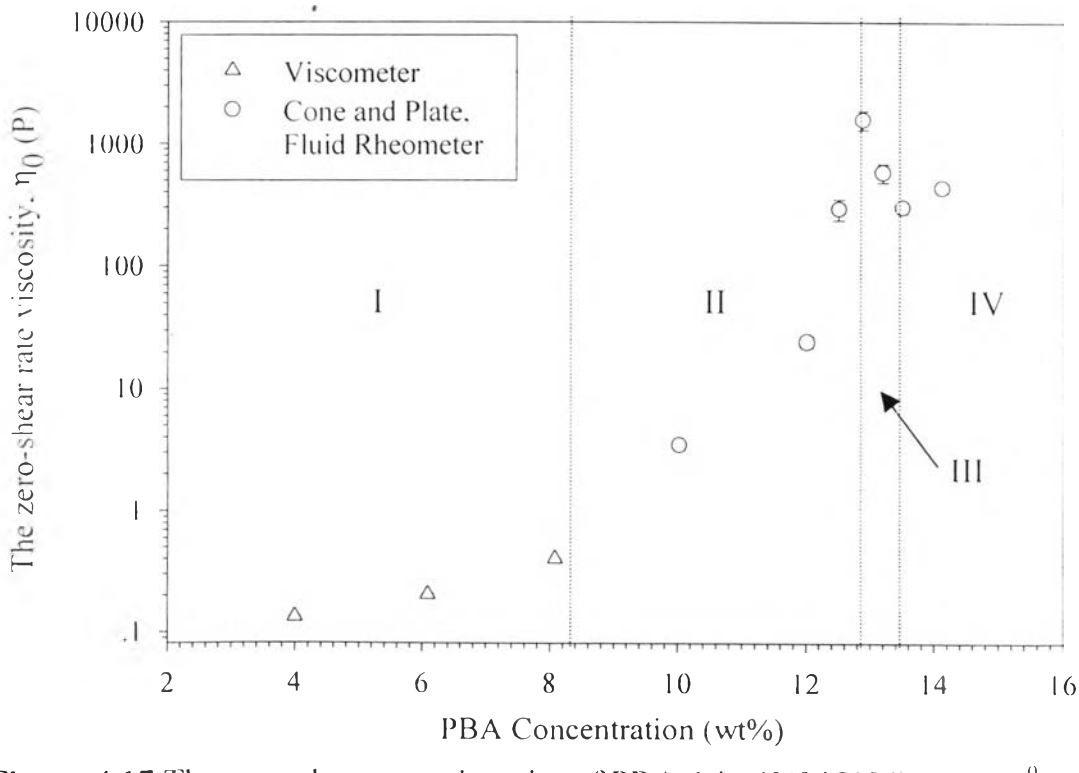

Figure 4.17 The zero-shear rate viscosity of PBA-1 in 4%LiCl/NMP at 25^0C.

4.2.1.2*Optical Textures*

The LC phase morphology of PBA solutions was studied by the optical polarizing microscope with crossed polars. Normally, the LC solution of aromatic polyamides is nematic. The nematic LC structure is ordered in one dimension (Figure 4.18(a)). The long axes of the molecules remain parallel, but the position of the centers of mass is randomly distributed. There is an orientation order, but no position order. So it is thread-like structure as shown in Figure 4.19. (Kroschwiz and Mary, 1995; Mark *et al.*, 1987; and Savyer and Grubb, 1996). The polarized optical micrographs of PBA-2 in 4%LiCl/DMAc, PBA-2 in 4%LiCl/NMP, PBA-1 in 4%LiCl/DMAc and PBA-1 in 4%LiCl/NMP with different concentrations at 25^0C are shown in Figures 4.20, 4.21, 4.22 and 4.23, respectively. With no material or with an isotropic material the field of view will be dark in crossed polars. Whereas optically anisotropic or birefringent material appears bright between crossed polars (Saver and Grubb, 1996). PBA-2 in both solvents, at concentrations below and above 4 wt% formed isotropic and anisotropic phase showing totally dark views (Figures 4.20(a) and 4.21(a)) and some bright views (Figures 4.20(b), 4.20(c), 4.20(d), 4.21(b), 4.21(c) and 4.21(d)), respectively. Also PBA-1 in both solvents, at concentrations below and above 8 wt% formed isotropic and anisotropic phase due to showing totally dark views (Figures 4.22(a) and 4.23(a)) and some bright views (Figures 4.22(b), 4.22(c), 4.22(d), 4.23(b), 4.23(c) and 4.23(d)), respectively. Figures 4.20(b), 4.21(b), 4.22(b) and 4.23(b) show dark views more than bright views. Figures 4.20(c), 4.21(c), 4.22(c) and 4.23(c) show bright views more than dark views. However, both of them are the biphasic phase. The former formed isotropic phase more than anisotropic phase, the latter formed anisotropic phase more than isotropic phase. Finally, Figures 4.20(d), 4.21(d), 4.22(d) and 4.23(d) show almost bright views. So PBA solution in this region formed fully LC phase. In this region, polymers form thread-like structures as can be observed

by comparing their polarized optical micrographs in Figure 4.19. We can summarize that, both PBA-1 and PBA-2 form nematic LC phase in 4%LiCl/DMAc and 4%LiCl/NMP solvents at 25^0C.

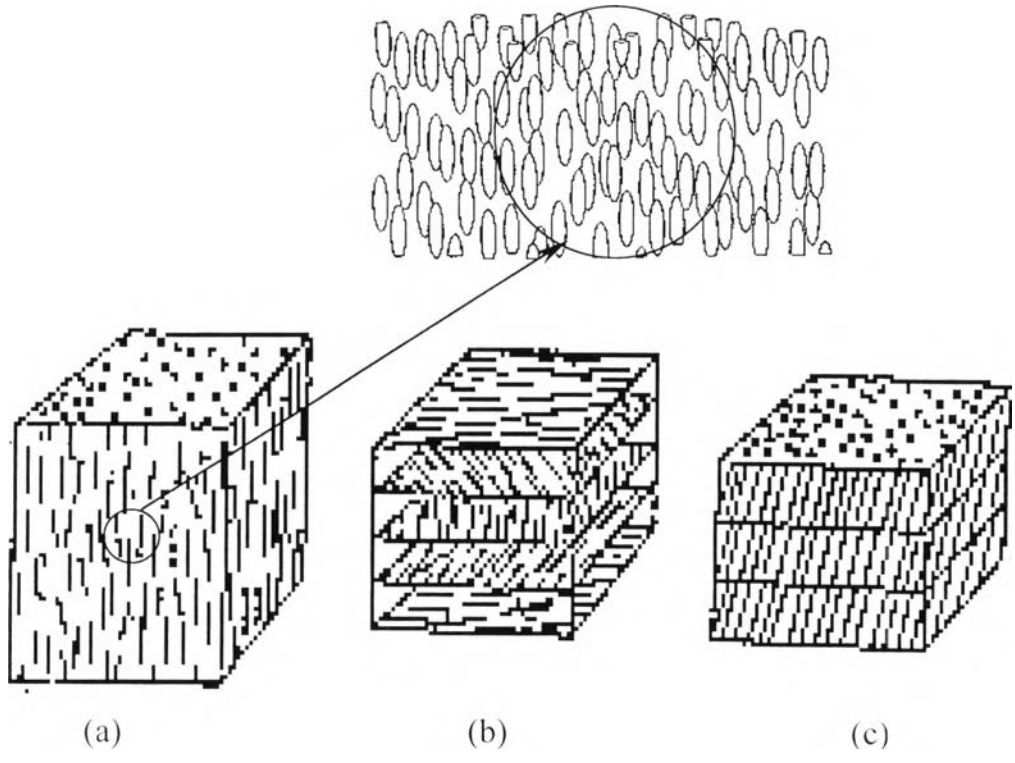

Figure 4.18 Structure of (a) nematic , (b) cholesteric , and (c) smectic C phase ((Kroschwiz and Mary, 1995 and Mark *et al.*, 1987).

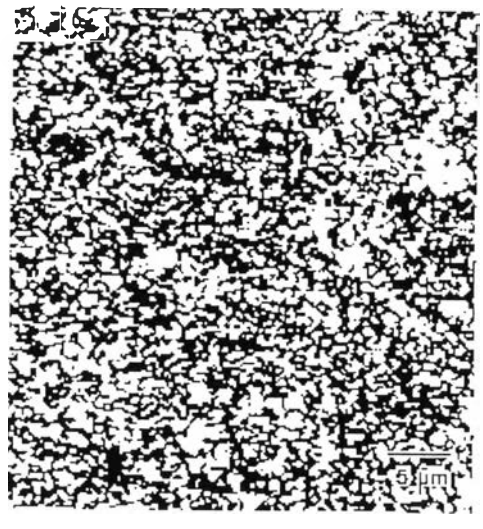

Figure 4.19 A polarized light micrograph of a sectioned nematic thermotropic LC polymer reveals a schlieren texture (Savyer and Grubb, 1996).

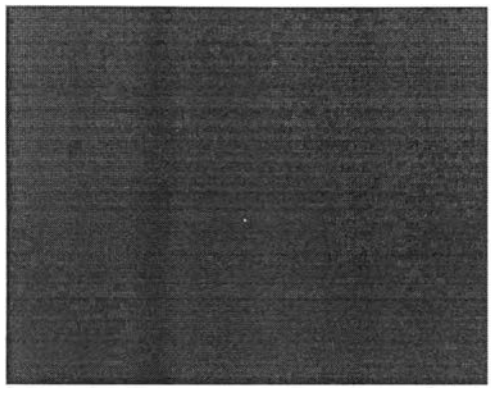

(a1) 1.01 wt%, 100X

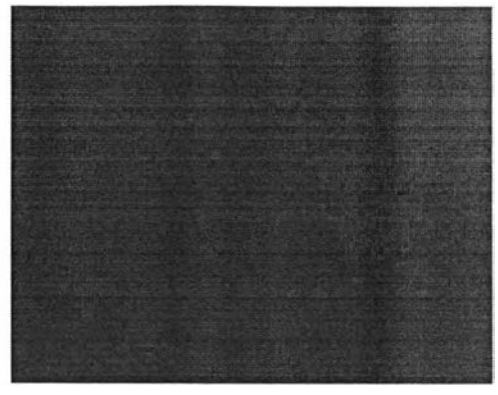

(a2) 2.02 wt%, 100X

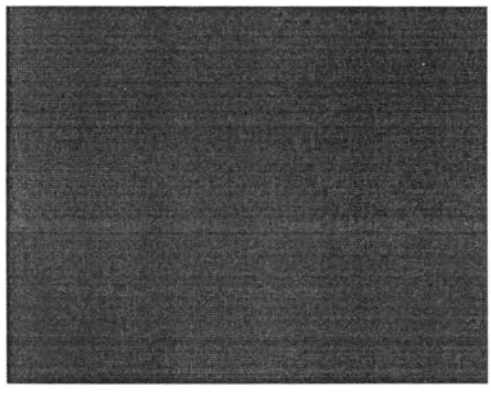

(a3) 3.03 wt%, 100X

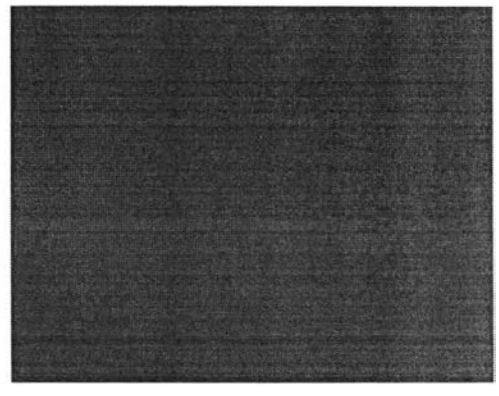

(a4) 3.79 wt%, 100X

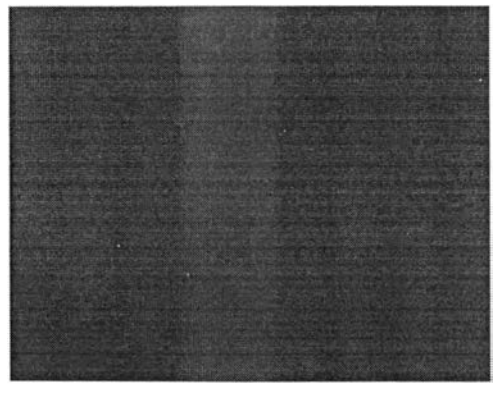

(a5) 4.00 wt%, 100X

(a) Isotropic Phase

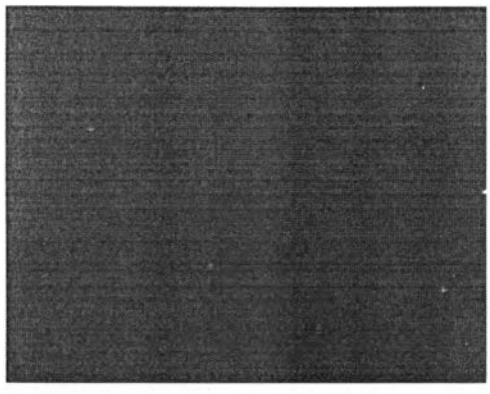

(b1) 4.26 wt%, 100X

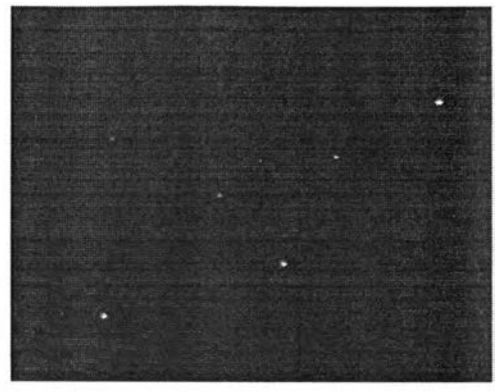

(b2) 4.30 wt%, 100X

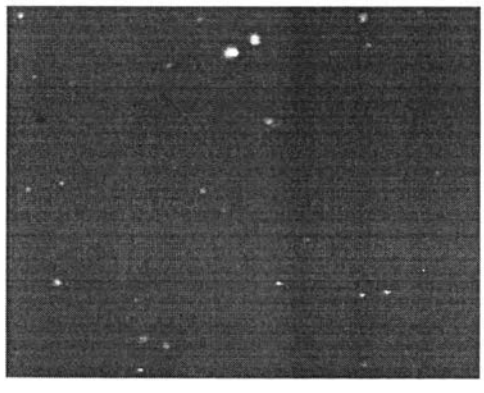

(b3) 4.45 wt%, 100X

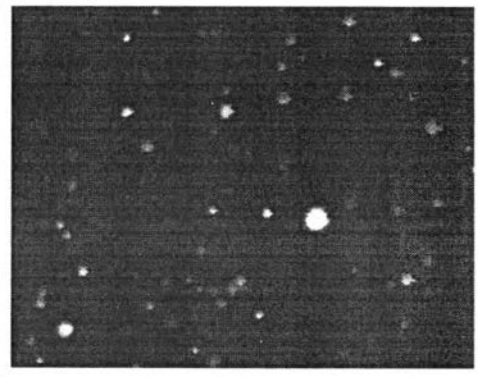

(b4) 4.53 wt%, 100X

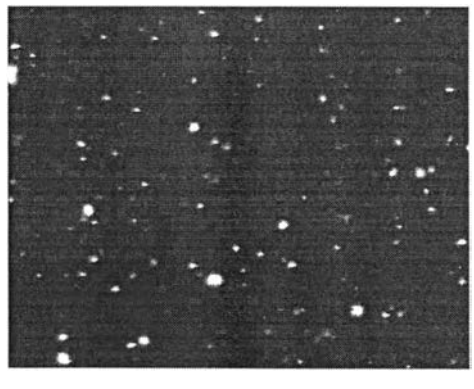

(b5) 5.15 wt%, 100X

(b) Biphasic Phase (Anisotropic phase in Isotropic phase)

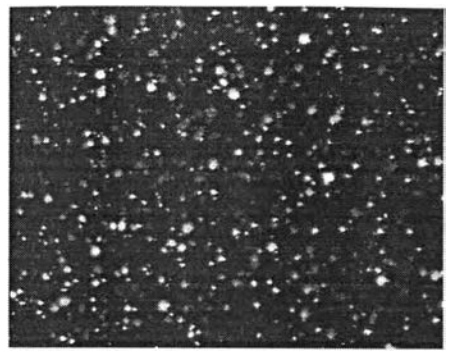

5.55 wt%, 100X

(c) Biphasic Phase (Isotropic phase in anisotropic phase)

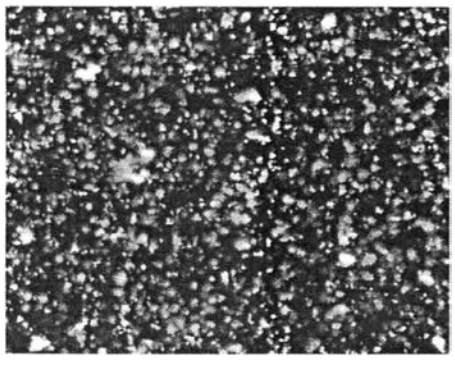

(d1) 6.10 wt%, 100X

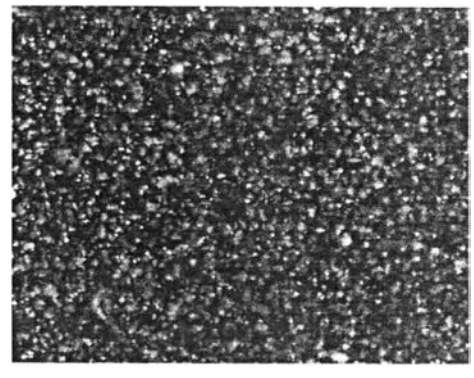

(d2) 7.09 wt%, 100X

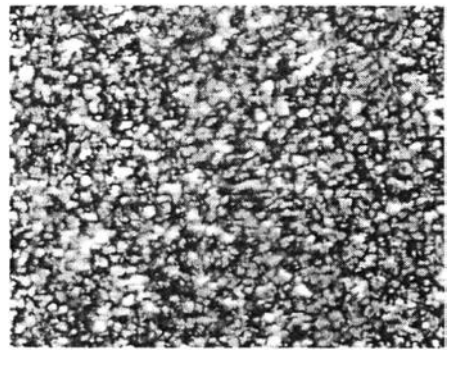

(d3) 8.10 wt%, 200X

(d) Fully LC Phase

Figure 4.20 Polarized optical micrographs of PBA-2 in 4%LiCl/DMAc at 25^0C with different concentrations: (a) Isotropic phase, C = 1.01-4.00 wt%; (b) Biphasic phase, C = 4.26-5.15 wt%; (c) Biphasic phase, C = 5.55 wt%; and (d) Fully LC phase, C = 6.10-8.10 wt%.

(a1) 1.01 wt%, 100X

(a2) 2.01 wt%, 100X

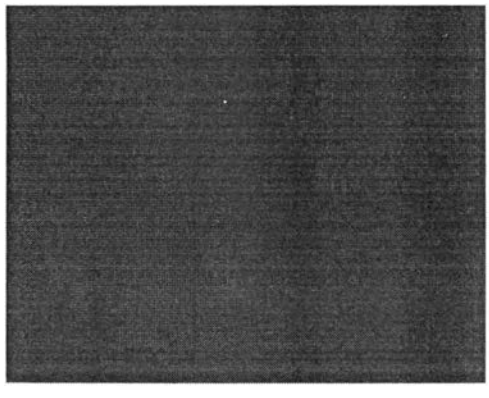

(a3) 3.08 wt%, 100X

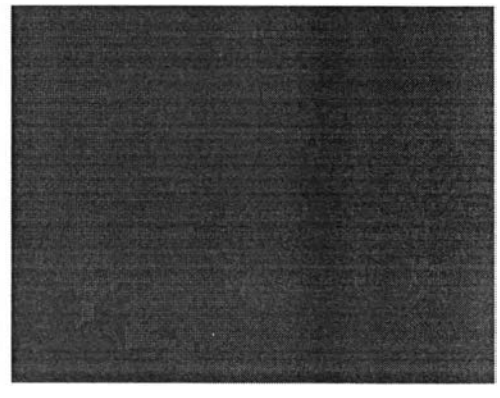

(a4) 4.02 wt%, 100X

(a) Isotropic Phase

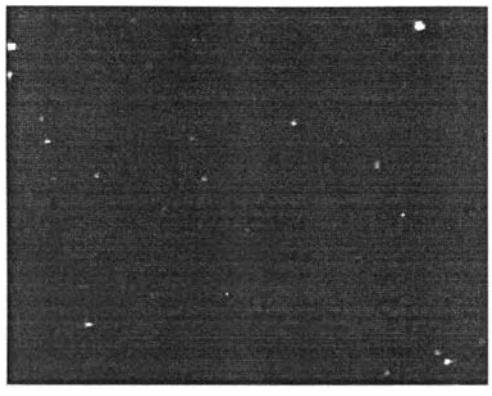

(b1) 4.25 wt%, 100X

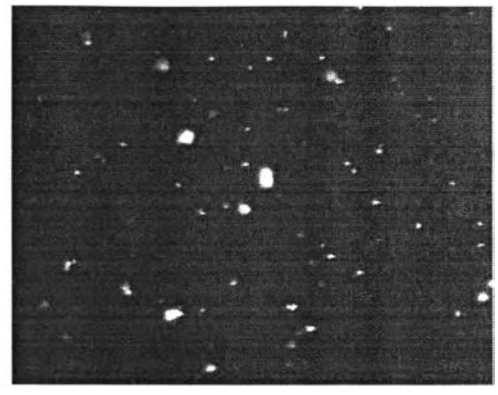

(b2) 4.44 wt%, 100X

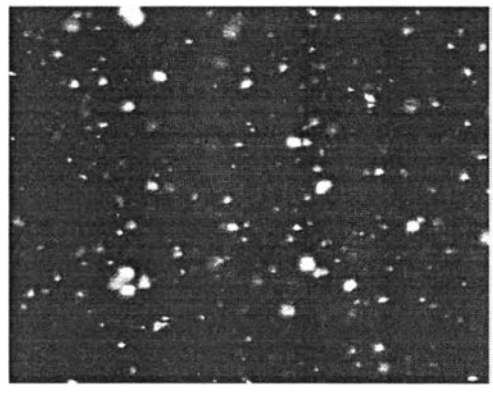

(b3) 5.12 wt%, 100X

(b) Biphasic Phase (Anisotropic phase in Isotropic phase)

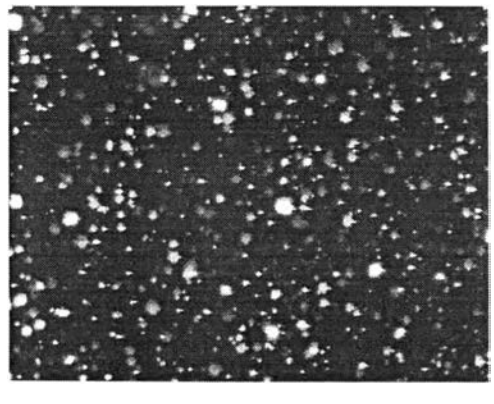

5.34 wt%, 100X

(c) Biphasic Phase (Isotropic phase in anisotropic phase)

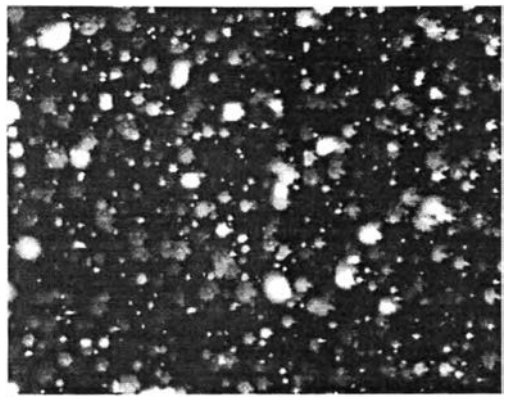

(d1) 5.61 wt%, 100X

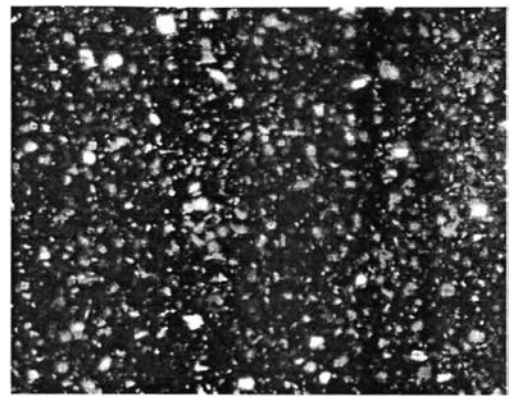

(d2) 6.05 wt%, 100X

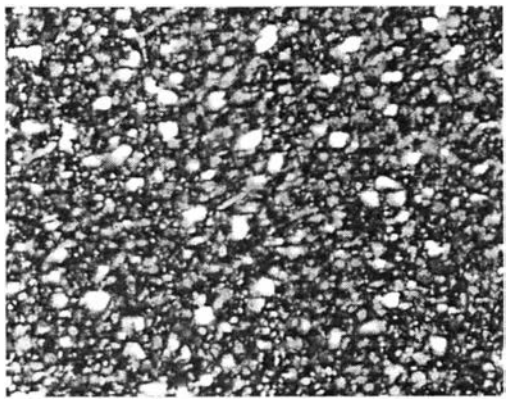

(d3) 7.01 wt%, 200X

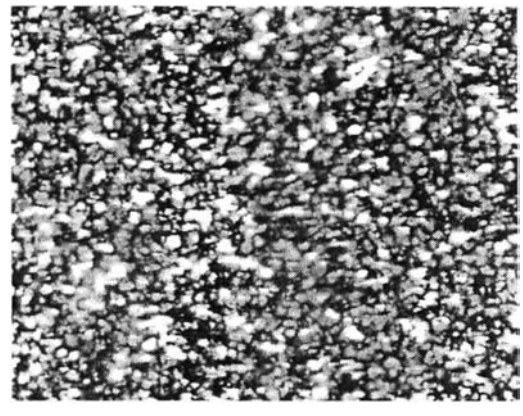

(d4) 8.06 wt%, 200X

(d) Fully LC Phase

Figure 4.21 Polarized optical micrographs of PBA-2 in 4%LiCl/NMP at 25^0C with different concentrations: (a) Isotropic phase, C = 1.01-4.02 wt%; (b) Biphasic phase, C = 4.25-5.12 wt%; (c) Biphasic phase, C = 5.34 wt%; and (d) Fully LC phase, C = 5.61-8.06 wt%.

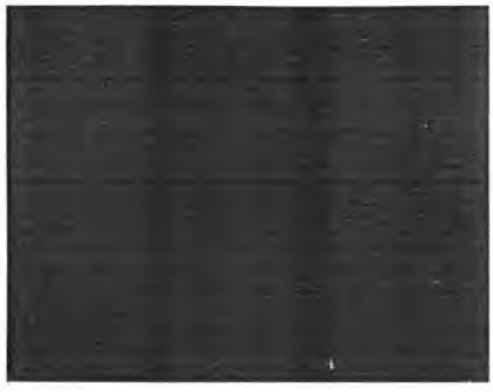

(a1) 4.01 wt%, 100X

(a2) 6.04 wt%, 100X

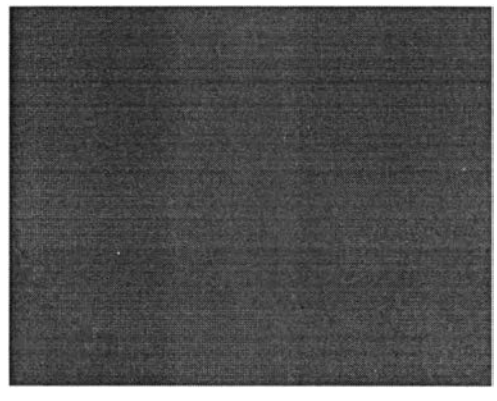

(a3) 8.05 wt%, 100X

(a) Isotropic Phase

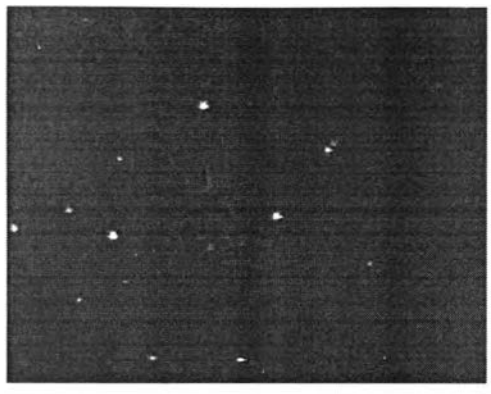

(b1) 9.99 wt%, 100X

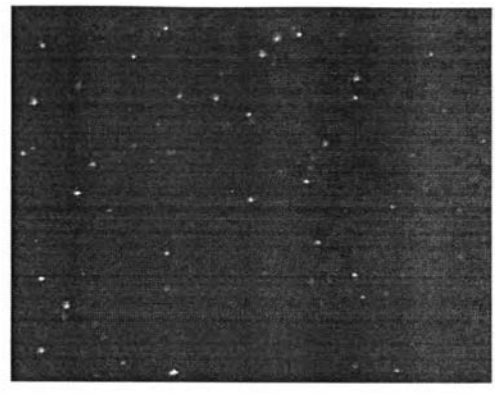

(b2) 11.99 wt%, 100X

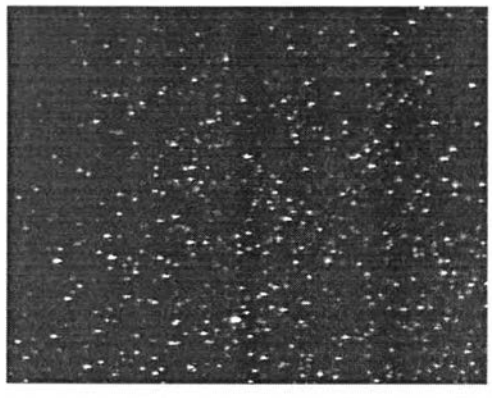

(b3) 12.5 wt0%, 100X

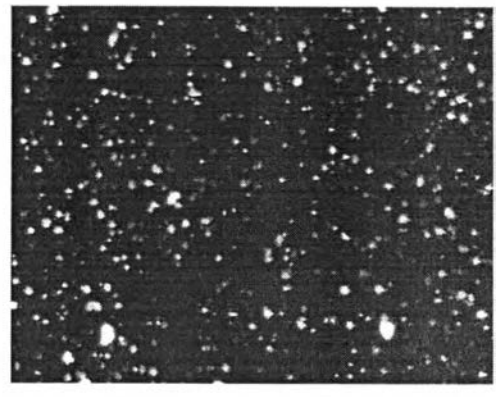

(b4) 13.04 wt%, 100X

(b) Biphasic Phase (Anisotropic phase in Isotropic phase)

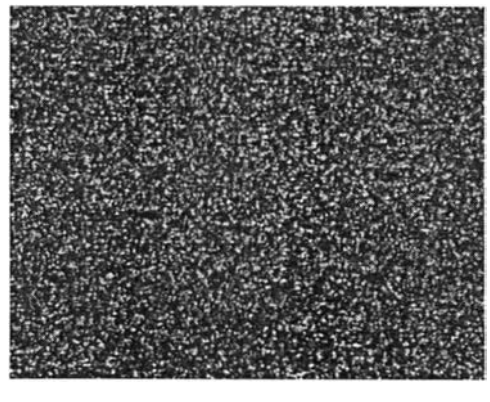

13.50 wt%, 100X

(c) Biphasic Phase (Isotropic phase in anisotropic phase)

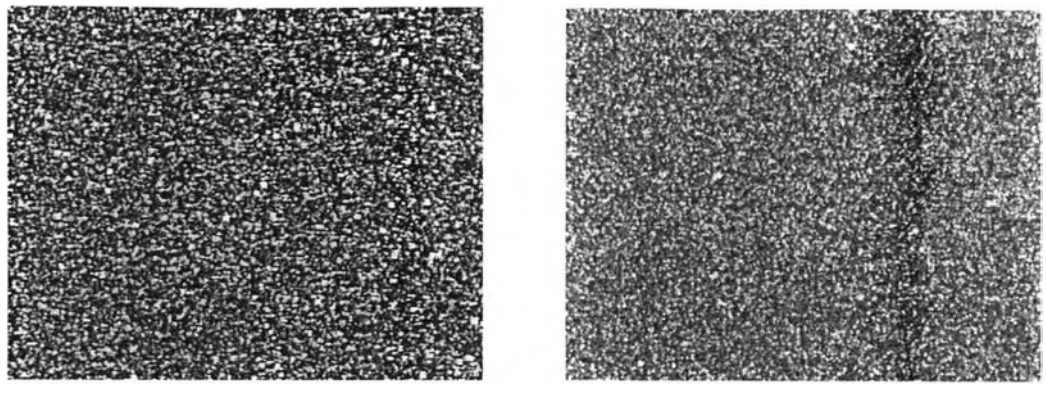

(d1) 14.16 wt%, 200X (d2) 15.06 wt%, 200X

(d) Fully LC Phase

Figure 4.22 Polarized optical micrographs of PBA-1 in 4%LiCl/DMAc at 25^0C with different concentrations: (a) Isotropic phase, C = 4.01-8.05 wt%; (b) Biphasic phase, C = 9.99-13.04 wt%; (c) Biphasic phase, C = 13.50 wt%; and (d) Fully LC phase, C = 14.16 and 15.06 wt%.

4.2.2 The Effect of Molecular Weight

The isotropic-nematic transition is a function of temperature and molecular weight. This transition occurs at lower concentrations at a higher molecular weight (Salamone, 1996). Figures 4.24 and 4.25 show the zero-shear rate viscosity at 25^0C as a function of PBA concentration in 4%LiCl/DMAc and 4%LiCl/NMP solvents, respectively. The higher the molecular weight of polymer, the lower the movement of polymer chain, the higher the viscosity and the easier the LC phases are formed. In both solvents, the viscosity of PBA-2 is higher than PBA-1. And the isotropic-nematic transition of PBA-2 occurs at lower concentration than PBA-1 as evidenced by shifting of concentration from 8 wt% to 4 wt%. This phenomenon is confirmed by optical textures (Figures 4.20-4.23). In addition, the optical textures of PBA-1 and PBA-2 in both solvents appear similar except their size scale. PBA-1 shows a smaller size scale.

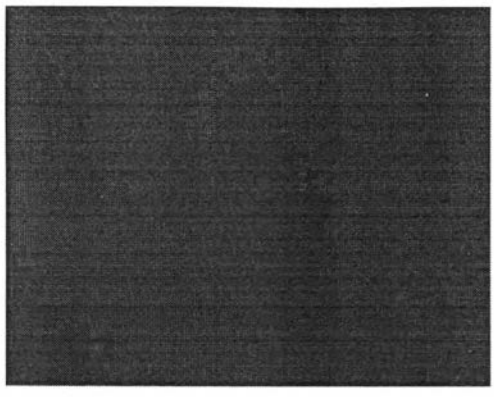

(a1) 4.00 wt%, 100X

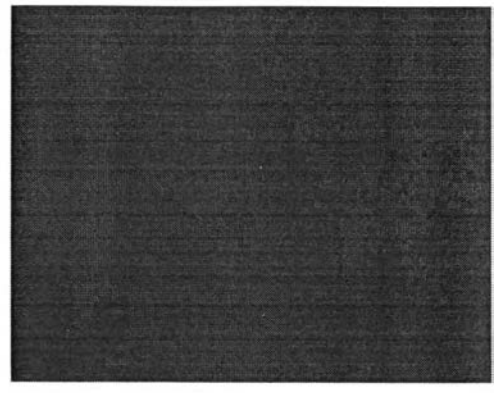

(a2) 6.09 wt%, 100X

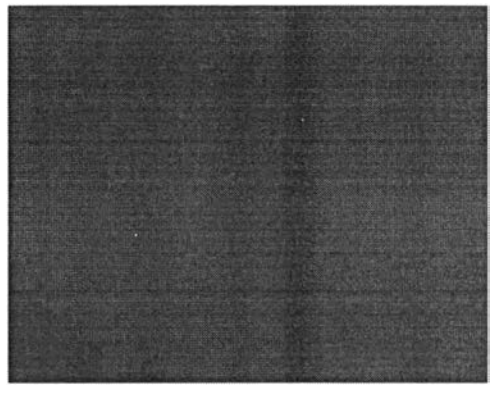

(a3) 8.08 wt%, 100X

(a) Isotropic Phase

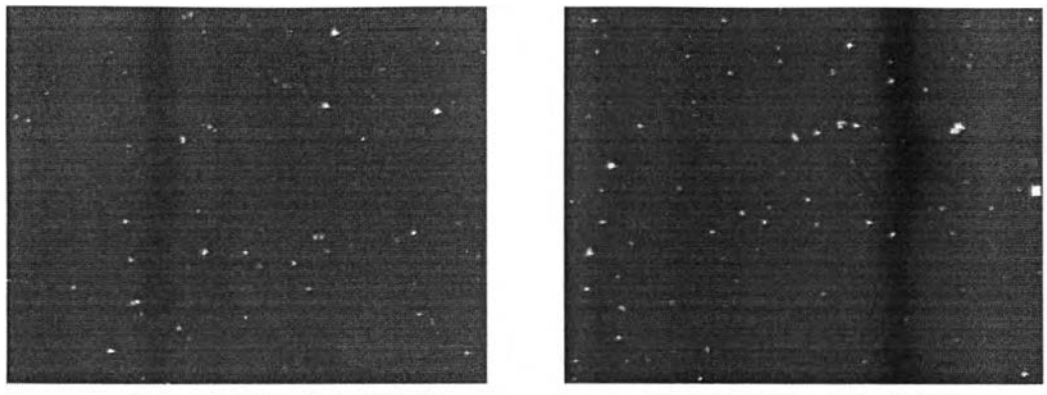

(b1) 10.03 wt%, 100X

(b2) 12.02 wt%, 100X

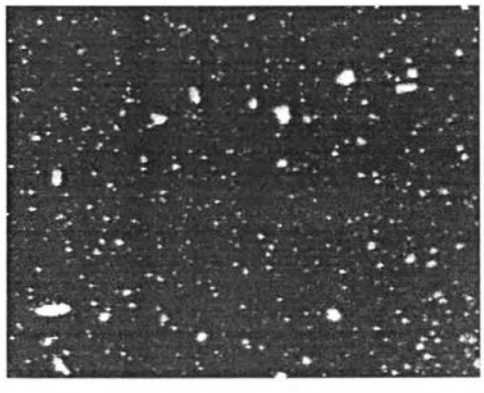

(b3) 12.52 wt%, 100X

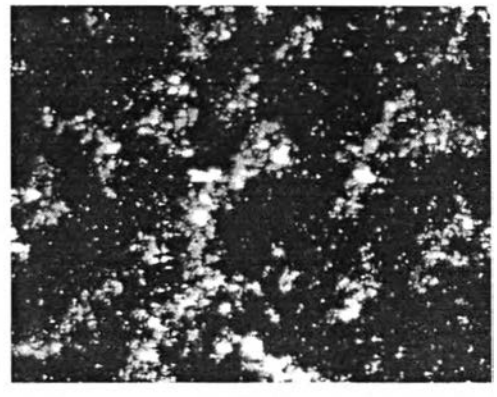

(b4) 12.89 wt%, 100X

(b) Biphasic Phase (Anisotropic phase in Isotropic phase)

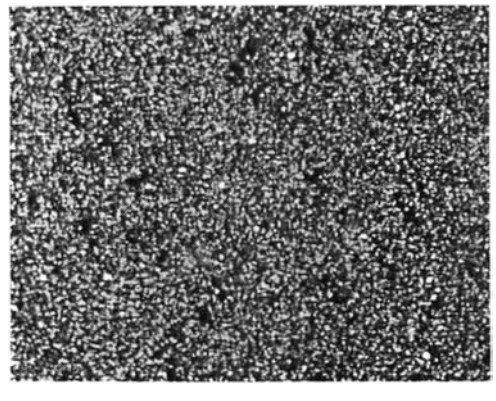

13.20 wt%, 100X

(c) Biphasic Phase (Isotropic phase in anisotropic phase)

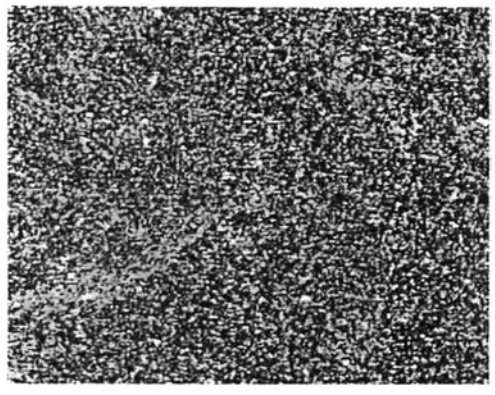

(d1) 13.51 wt%, 200X

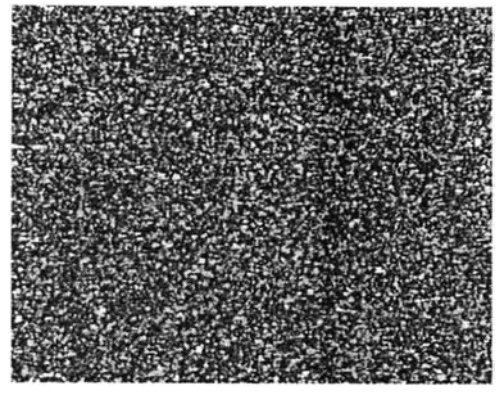

(d2) 14.15 wt%, 200X

(d) Fully LC Phase

Figure 4.23 Polarized optical micrographs of PBA-1 in 4%LiCl/NMP at 25^{0}C with different concentrations: (a) Isotropic phase, C = 4.00-8.08 wt%; (b) Biphasic phase, C = 10.13-12.89 wt%; (c) Biphasic phase, C = 13.20 wt%; and (d) Fully LC phase, C = 13.51-14.15 wt%.

4.2.3 The Effect of Polymer-Solvent Interaction

PBA is soluble in tertiary organic amides such as dimethylacetamide (DMAc), 1-methyl-2-pyrrolidone (NMP) and tetramethylurea containing lithium or calcium chloride, or in concentrated sulfuric acid, and hydrogen fluoride (Mark *et al.,* 1987). This experiment was carried in LiCl/DMAc and LiCl/NMP. Solubility in the amide-salt solvents results from association of chloride ions with the amide protons in the polymer; as indicated in Figure 4.26 (Mark *et al.,* 1987). Figures 4.27 and 4.28 show the zero-shear rate viscosity of PBA solutions at 25^{0}C in 4%LiCl/DMAc and 4%LiCl/NMP solvents for PBA-1 and PBA-2, respectively. PBA molecule in LiCl/NMP solvent system is more difficult to move than in LiCl/DMAc solvent system due to the bigger pendant positive group (Figure

4.26). The lower the movement of polymer chain, the higher the viscosity and the easier LC phase is formed. However, the molecular weight is more influential to the movement of polymer chain than the effect of solvent. In both molecular weights, PBA solutions in 4%LiCL/NMP in all regimes have slightly higher viscosity than in 4%LiCl/DMAc. In addition, PBA solutions in 4%LiCL/NMP for both molecular weights form LC phase easier due to the lower concentration in regimes III and IV. This phenomenon is confirmed by optical textures. The higher the bright views of PBA solution can be observed in 4%LiCL/NMP.

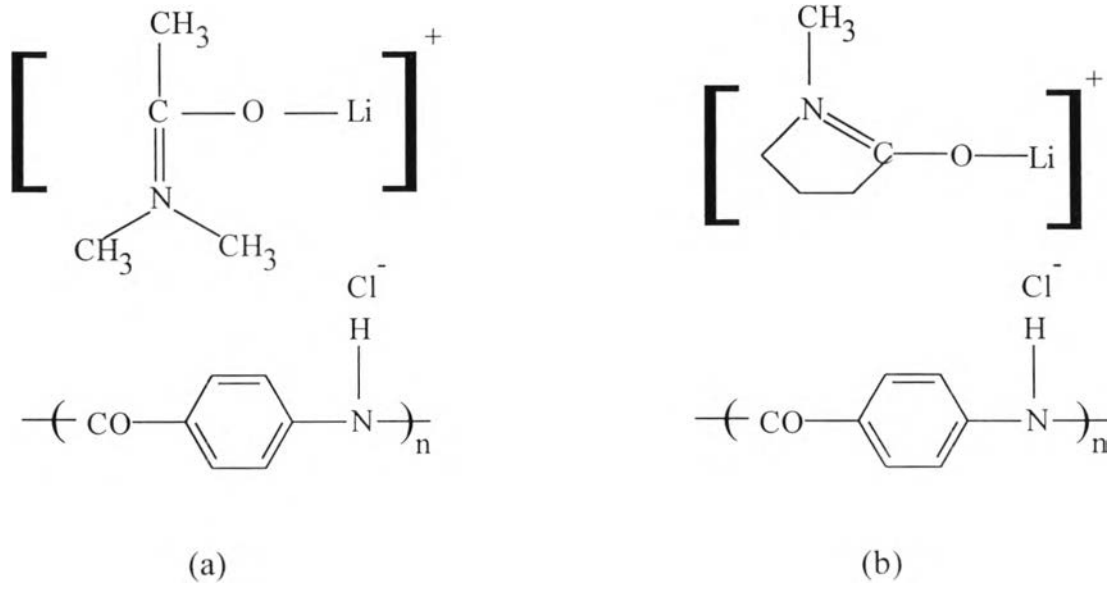

Figure 4.26 Postulated structure of solvated PBA in (a) LiCl/DMAc and (b) LiCl/NMP solvents.

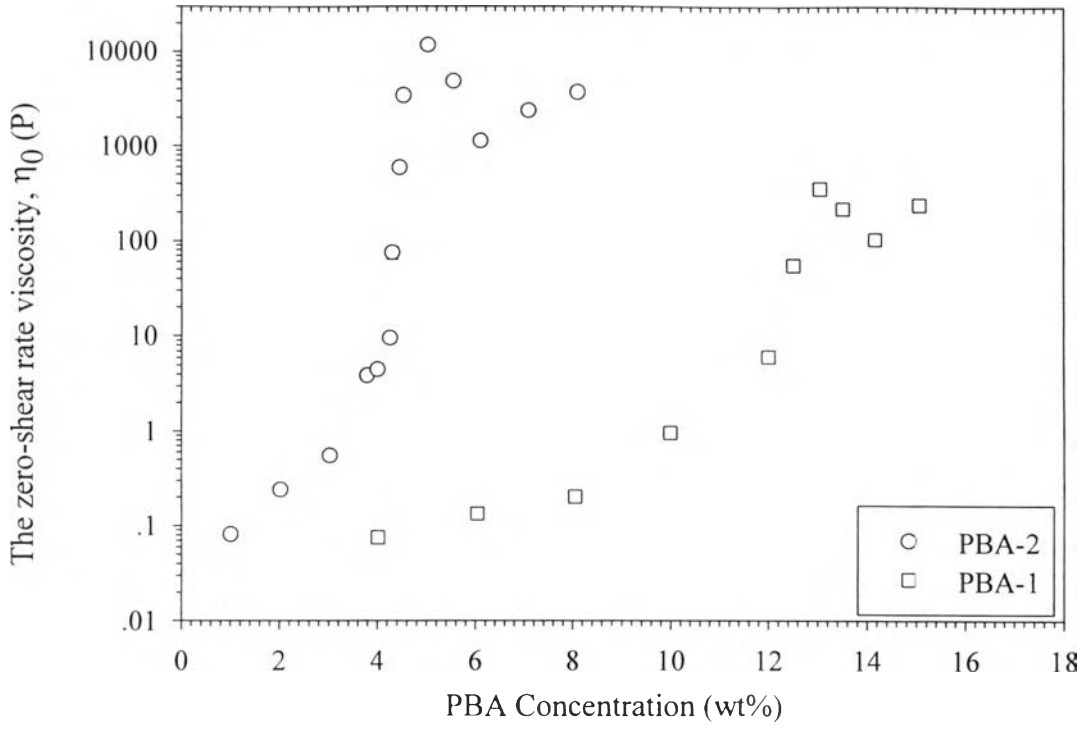

Figure 4.24 The zero-shear rate viscosity of PBA-1 and PBA-2 in 4%LiCl/DMAc at 25^0C.

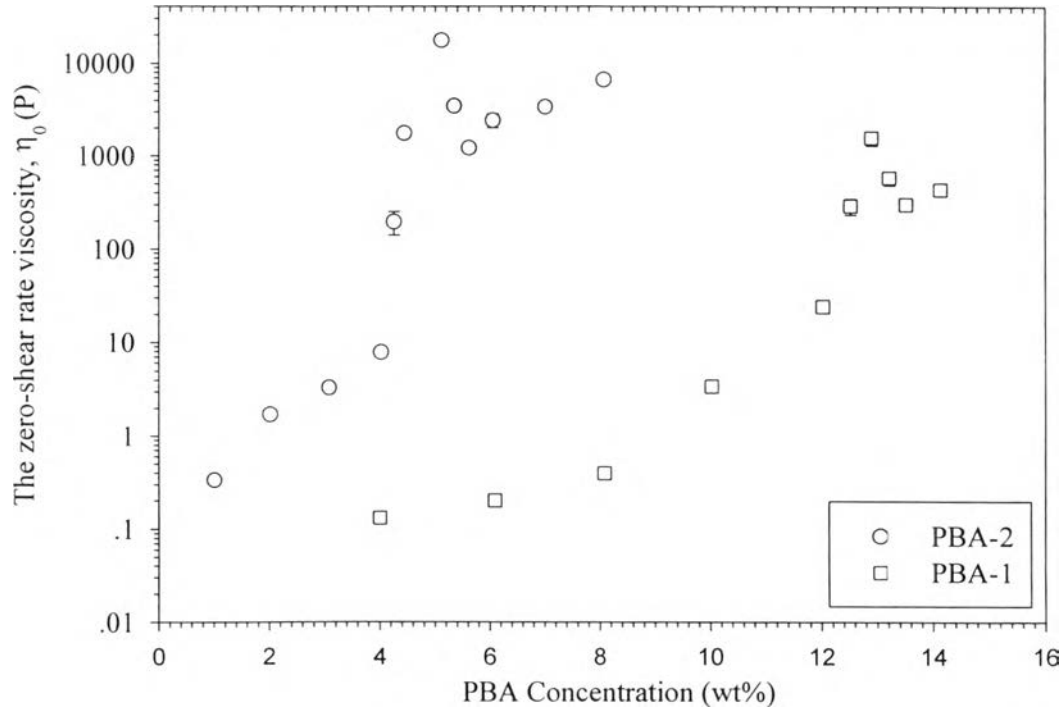

Figure 4.25 The zero-shear rate viscosity of PBA-1 and PBA-2 in 4%LiCl/NMP at 25^0C.

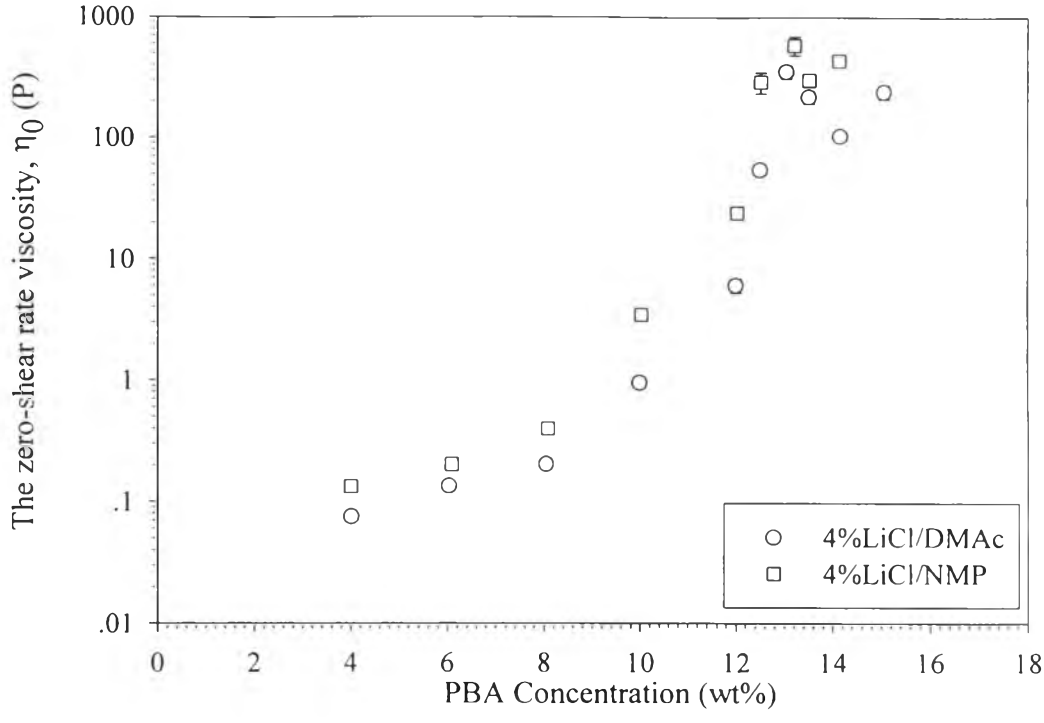

Figure 4.27 The rero-shear rate viscosityof PBA-1 in 4%LiCl/DMAc and 4%LiCl/NMP solvents at 25^{0}C.

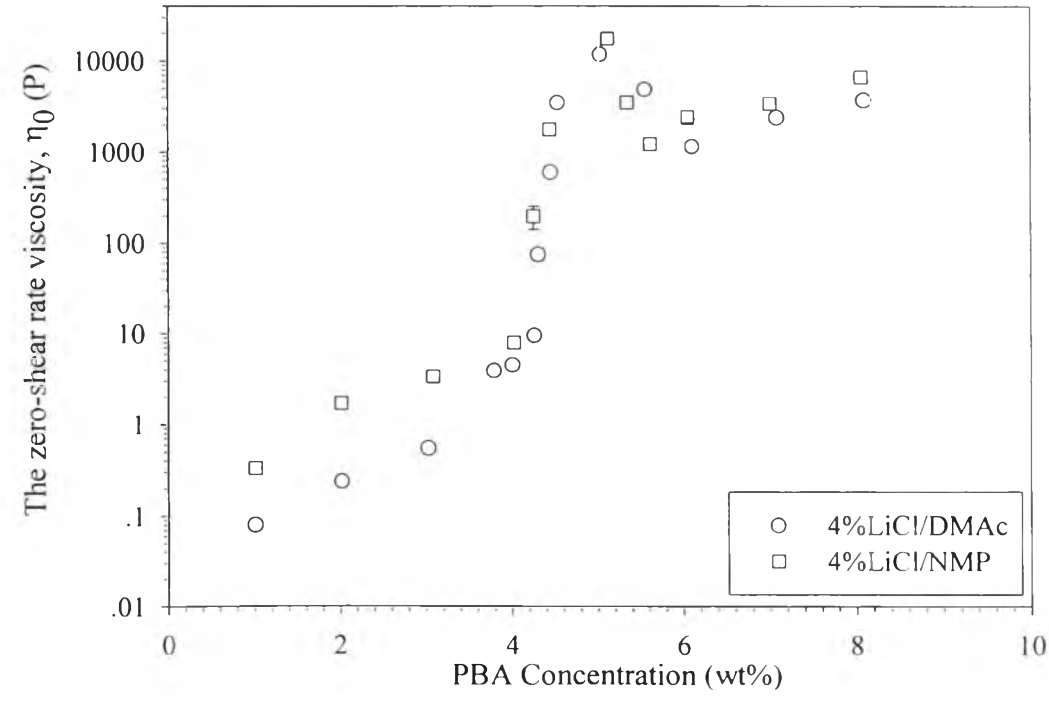

Figure 4.28 The rero-shear rate viscosityof PBA-2 in 4%LiCl/DMAc and 4%LiCl/NMP solvents at 25^{0}C.

The typical flow curve of LC polymers is schematically depicted in Figure 4.29.

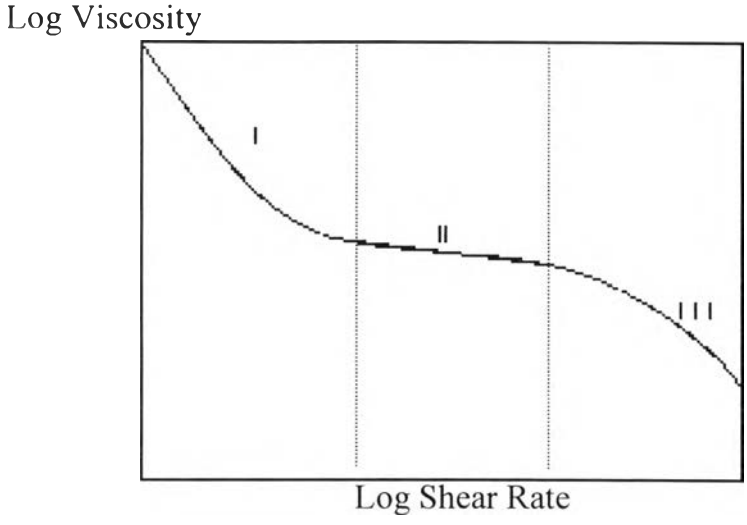

Figure 4.29. Typical flow curve of LC polymer.

A possible interpretation of the three-regime flow curve of LC polymers have been reported (Salamone, 1996), as shown in Figure 4.29. In the first regime, the flow does not change the polydomain structure, the director preserves its initial random orientation, and polymer needs high stress value (yield stress and high viscosity). In the second regime, the shear stress causes the disentangling of the polydomain texture giving rise to a dispersed polydomain structure. In this condition, the viscosity depends less on shear rate. At the third regime, the flow orients the director in a single direction, creating a monodomain . This monodomain structure flows easily along the shear direction (very low viscosity). Some flow curves of PBA solution for all systems are shown in Figures 4.30, 4.31, 4.32, and 4.33 (all flow curves for all systems are shown in Appendix C).

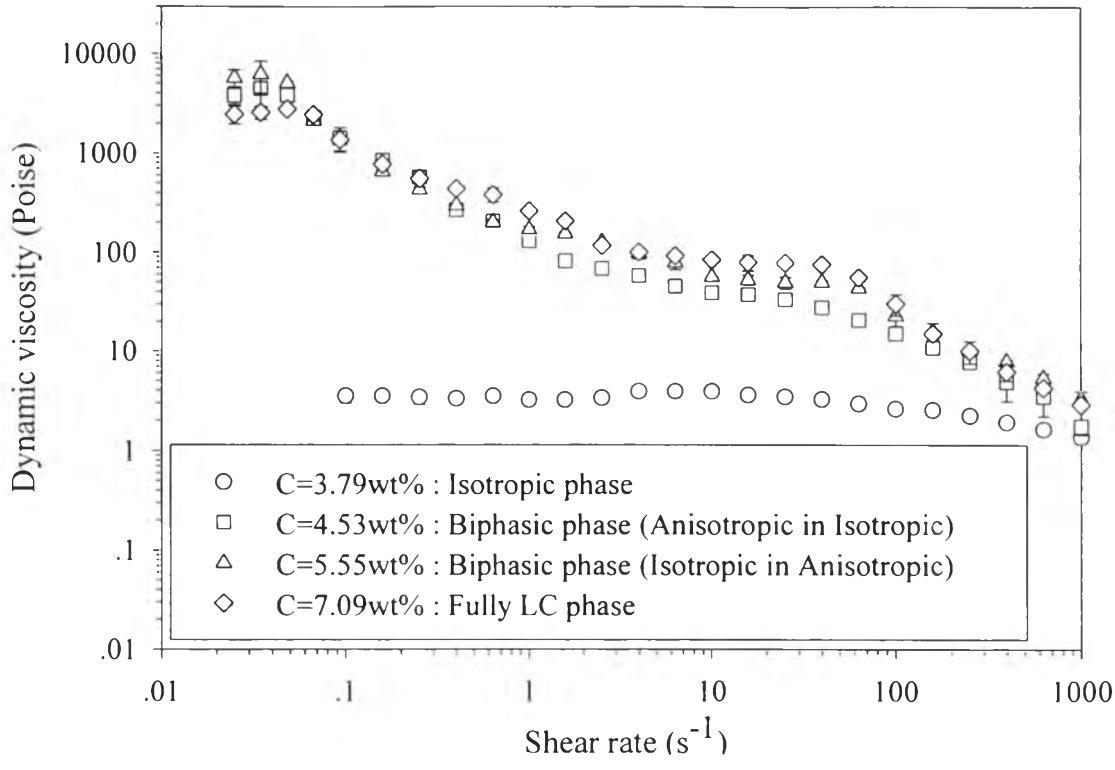

Figure 4.30 Some flow curves of PBA-2 in 4%LiCl/DMAc.

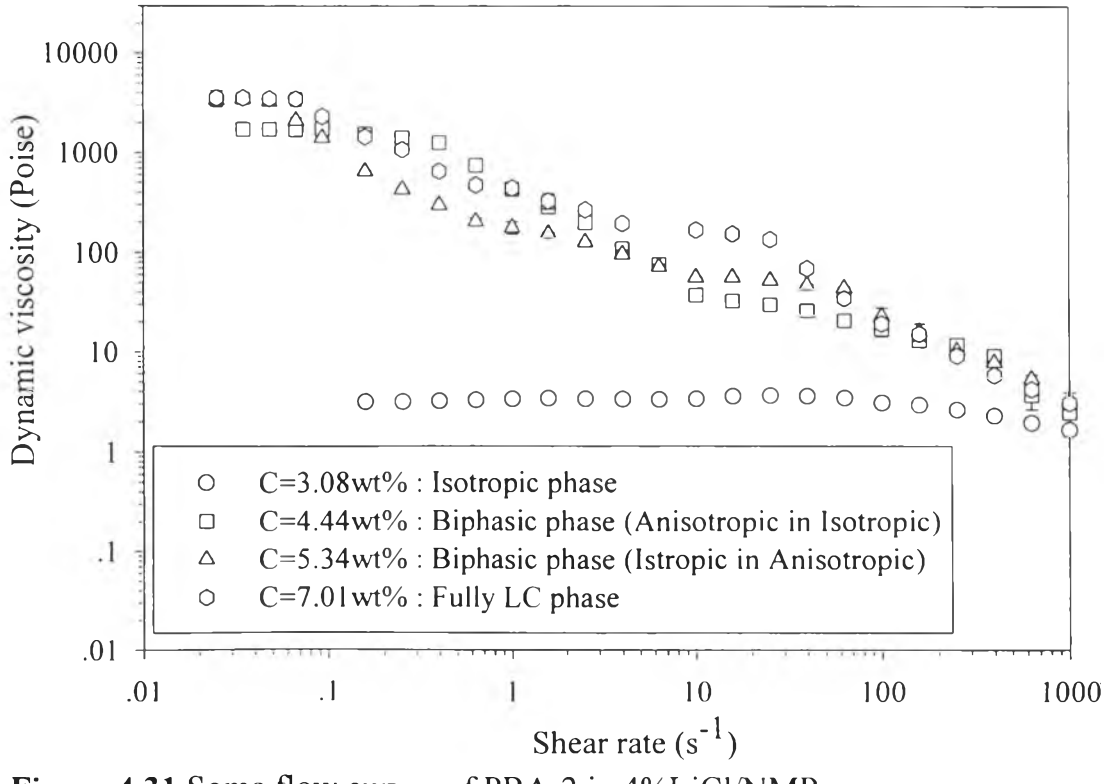

Figure 4.31 Some flow curves of PBA-2 in 4%LiCl/NMP.

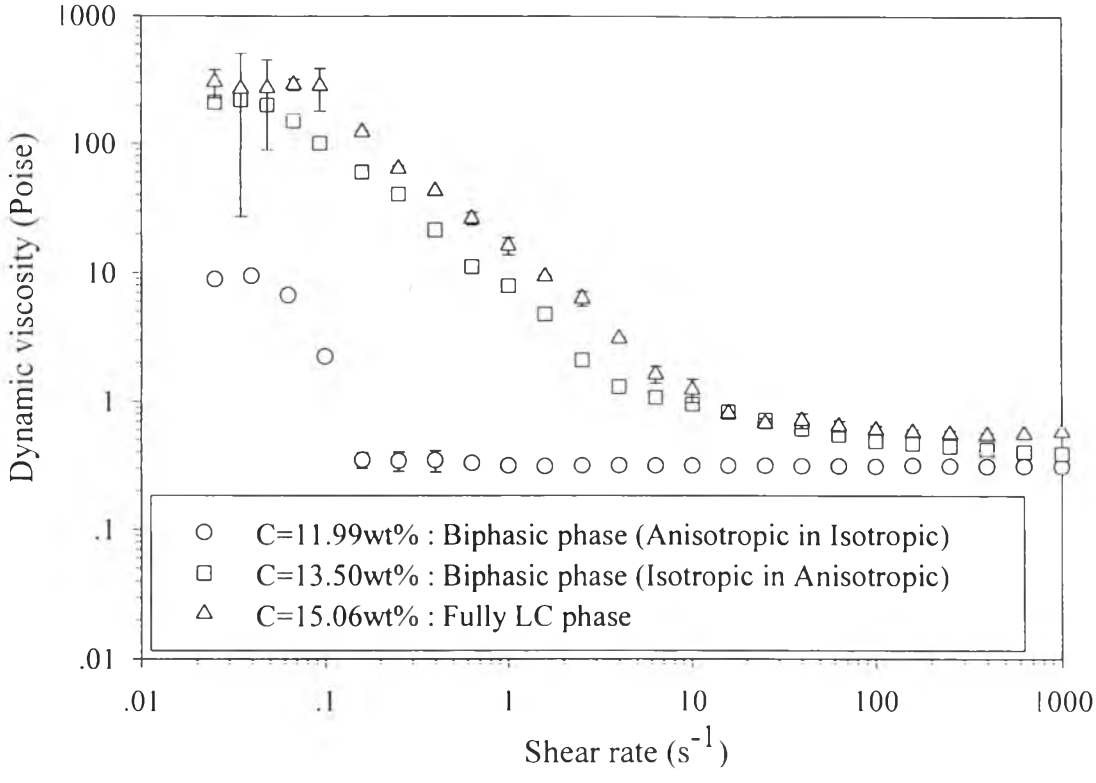

Figure 4.32 Some flow curves of PBA-1 in 4%LiCl/DMAc.

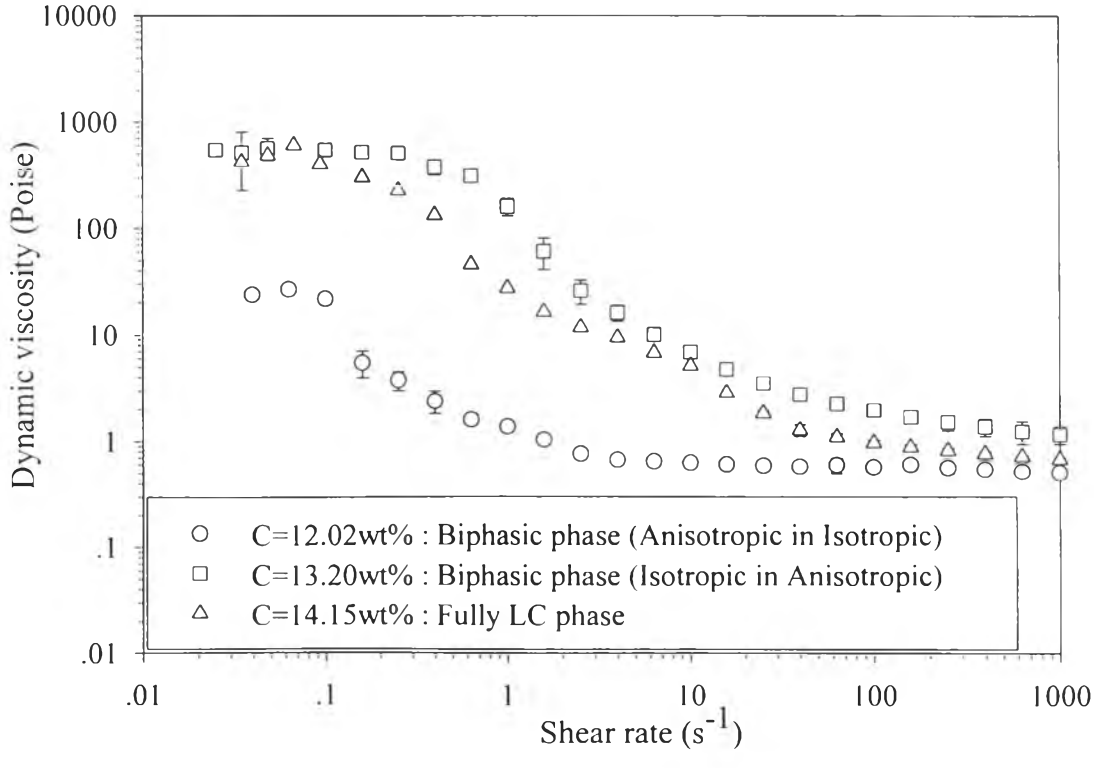

Figure 4.33 Some flow curves of PBA-1 in 4%LiCl/NMP.

From the flow curves of PBA-2 in both solvents, phases that are beyond isotropic phase appear all of the three-regime whereas isotropic phase does not show the first regime. This is because isotropic phase does not need a yield stress (that is the stress to be overcome to impose a flow to the system) at low shear rates (Salamone, 1996). From the curves of PBA-1 in both solvents, phases that are beyond isotropic phase appear only the first and the second regime. PBA-1 was forms only very small LC domains so it does not creat a monodomain structure.

In summary, PBA-1 and PBA-2 form nematic LC phases in 4%LiCl/DMAc and 4%LiCl/NMP solvents at 25^0C at very low concentration compared to other lyotropic LC polymers.

4.3 ER Measurement of PBA-1 Suspensions

The medium or the liquid phase that is used in the particle dispersion type of ER fluids should be a Newtonian fluid; its viscosity does not depend on shear rate. So the changes in viscosity or other rheological properties upon applying an electric field are due to the forming of chain-like or fibrillated structure in the suspension only, not form the medium (Mata, 2000). The viscosity of the 100 cSt silicone oil, which is used as a medium for ER fluid sample in this work, does not change with shear rate. So this silicone oil behaves like a Newtonian fluid (Mata, 2000). PBA-1 is used to be a dispersed phase because its particle size can be easily prepared to have a nearly monodisperse distribution (15 μm) and its particle shape is nearly spherical even without ball-milling (Appendix E). The ER measurement data of lyotropic LC fluid is shown in Appendix E.

A modified cone and plate fixture (as shown in Appendix D) was used with the gap size of 0.063 ± 1 mm. The electric field strengths (0, 0.02, 0.25, 0.4, 0.5,1 and 2 kV/mm) were applied to the fluids for 5 minutes in order to obtain an equilibrium chain-like or columnar structure before each measurement. All measurements were performed at 25 ± 0.1^{0}C and carried out at least two or three times. In order to obtain reproducible data, the ER fluid was redispersed prior to each measurement.

In this work, ER properties, in the linear and the nonlinear viscoelastic regimes of the 10 wt% PBA-1 in 100 cSt silicone oil measured, are the storage modulus (G') and the loss modulus (G'') as a function of the electric field strength and the results will be compared with those of the polyaniline suspension (Mata, 2000).

4.3.1 Effect of Strain Amplitude

This measurement was conducted at the frequency of 1 rad/s at various electric field strengths in order to determine the linear viscoelastic regime prior to the frequency sweep experiment.

Figure 4.34, 4.35, 4.36, 4.37, 4.38, 4.39 and 4.40 show G' and G'' dependence on %strain of 10 wt% PBA-1 suspension at the frequency of 1 rad/s at the electric field strengths of 2, 1, 0.5, 0.4, 0.25, 0.02 and 0 kV/mm, respectively.

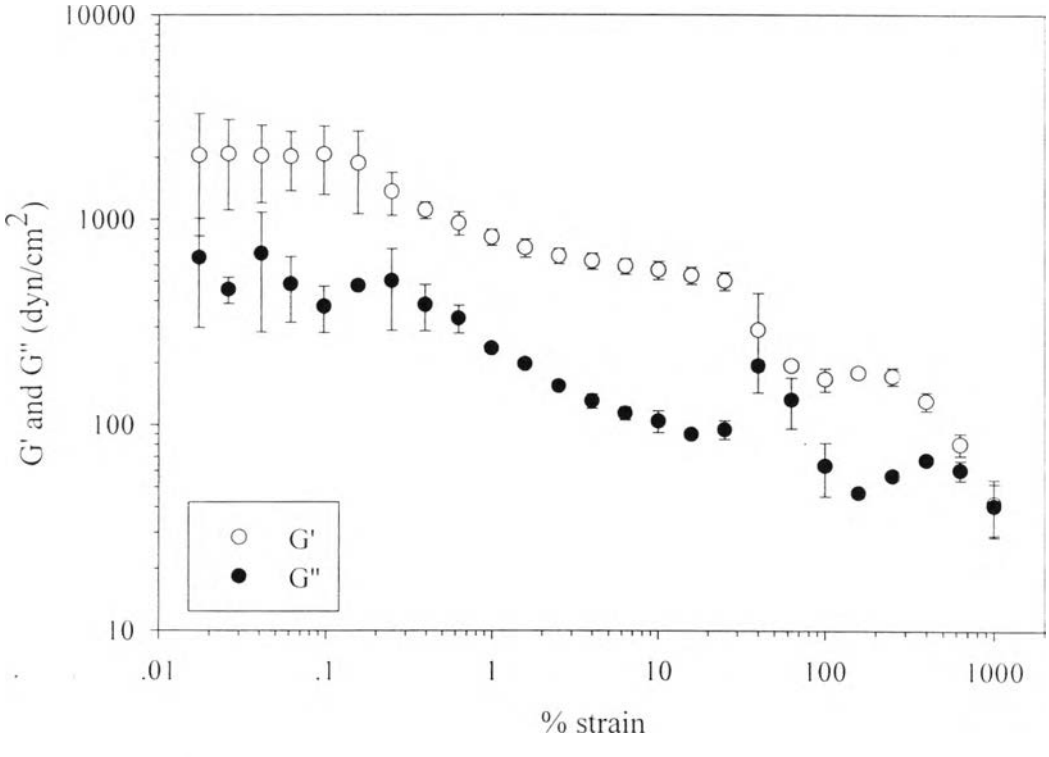

Figure 4.34 G' and G'' dependence on %strain of 10 wt% PBA-1 suspension at the electric field strength of 2 kV/mm.

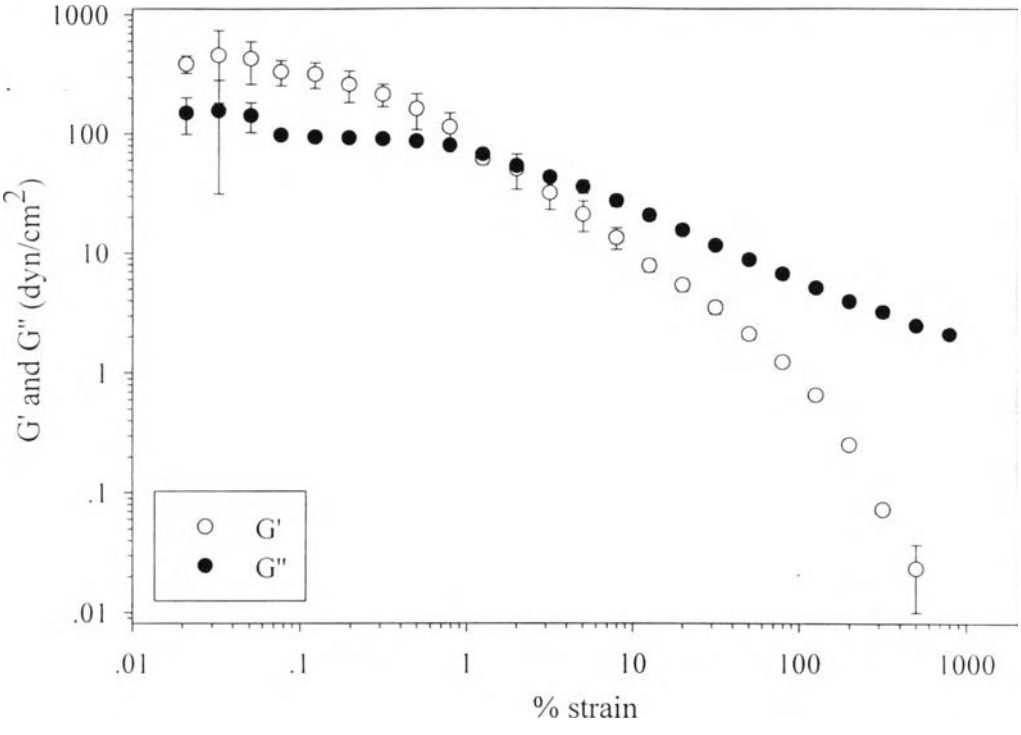

Figure 4.35 G` and G`` dependence on %strain of 10 wt% PBA-1 suspension at the electric field strength of 1 kV/mm.

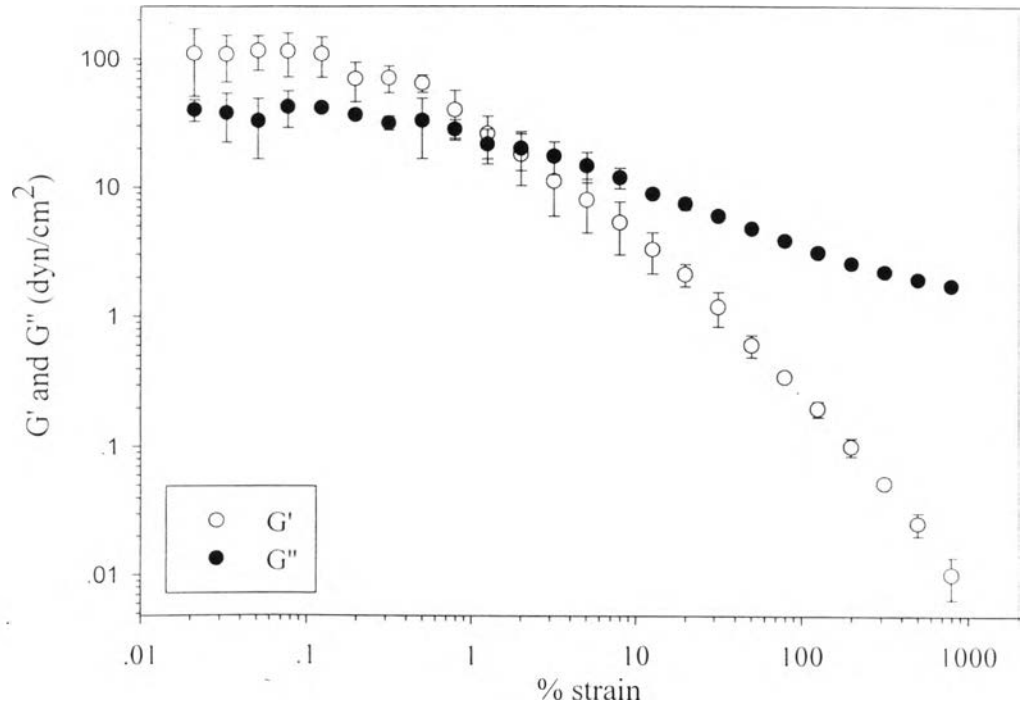

Figure 4.36 G` and G`` dependence on %strain of 10 wt% PBA-1 suspension at the electric field strength of 0.5 kV/mm.

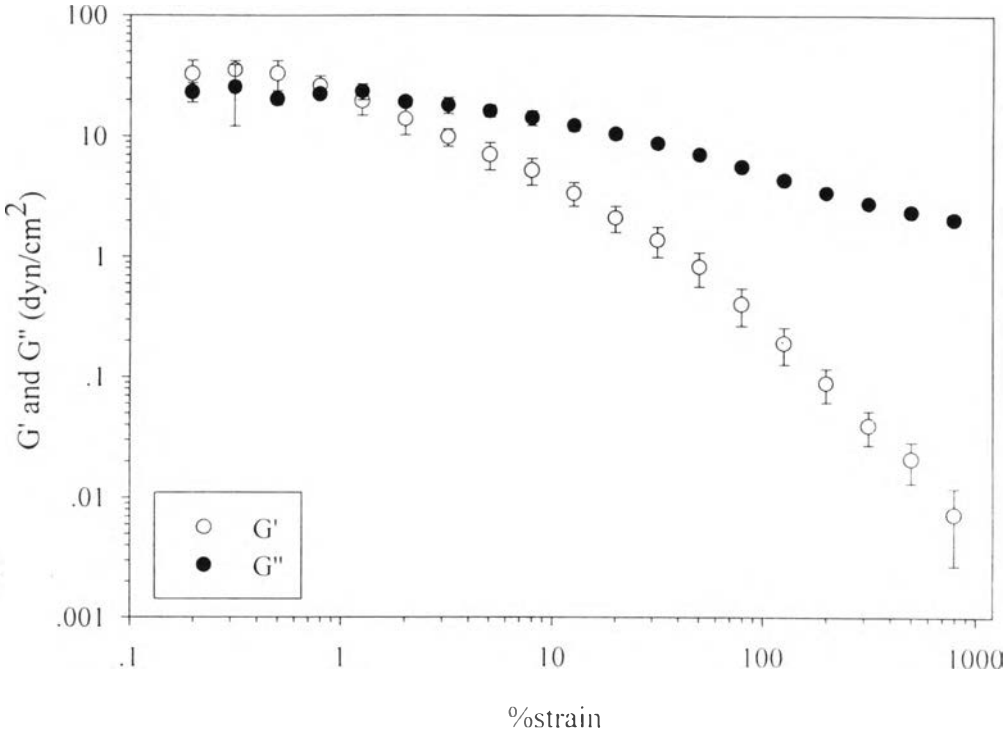

Figure 4.37 G' and G'' dependence on %strain of 10 wt% PBA-1 suspension at the electric field strength of 0.4 kV/mm.

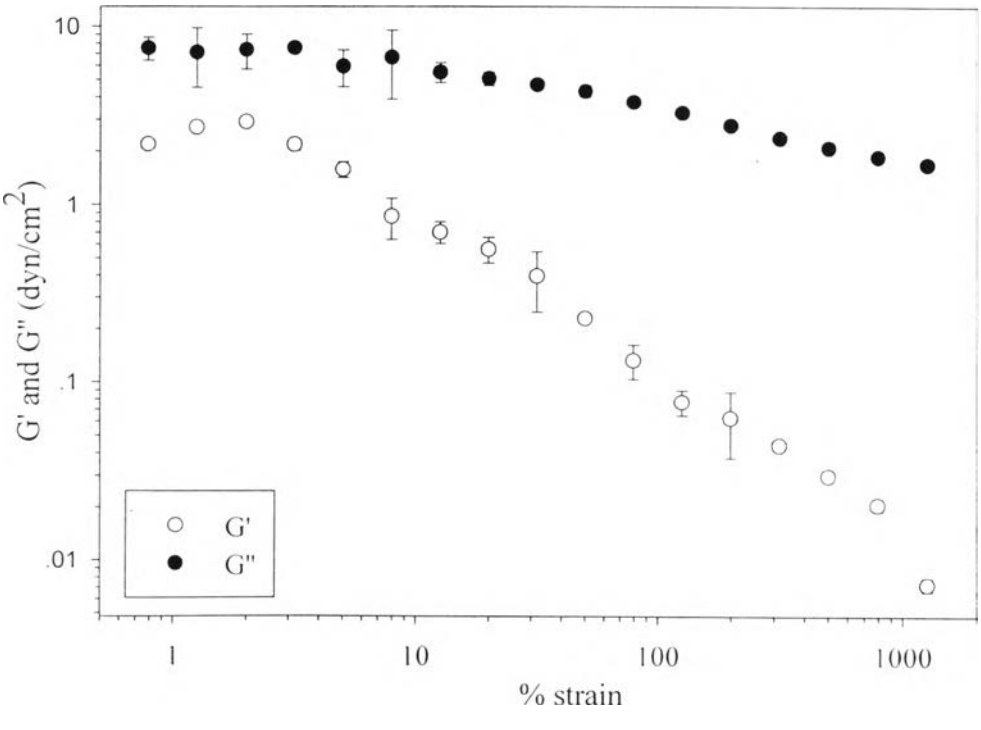

Figure 4.38 G' and G'' dependence on %strain of 10 wt% PBA-1 suspension at the electric field strength of 0.25 kV/mm.

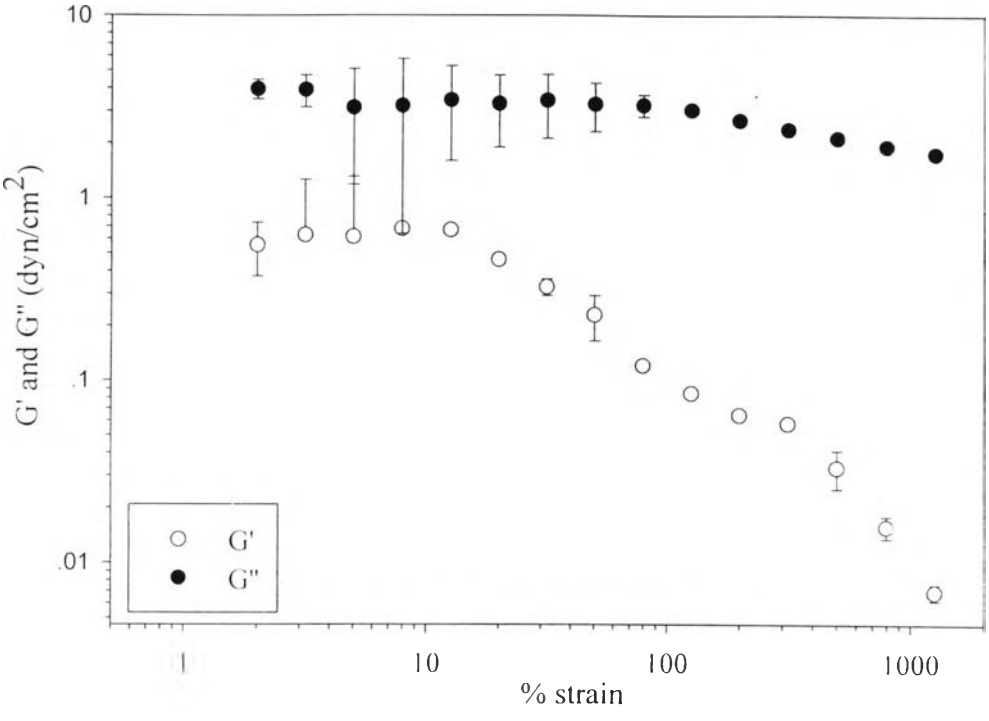

Figure 4.39 G' and G'' dependence on %strain of 10 wt% PBA-1 suspension at the electric field strength of 0.02 kV/mm.

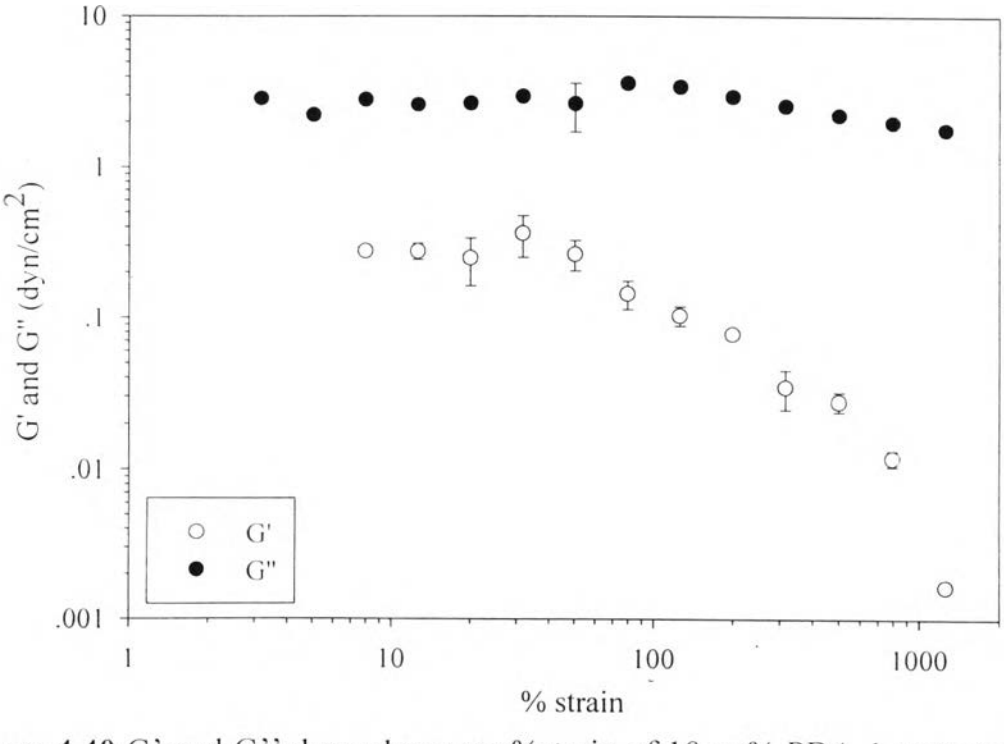

Figure 4.40 G' and G'' dependence on %strain of 10 wt% PBA-1 suspension at the electric field strength of 0 kV/mm.

For electric field strengths of 1, 0.5 and 0.4 kV/mm, G' are larger than G'' in the linear viscoelastic regime, where G' or G'' do not depend on %strain. The reverse trend can be observed in the nonlinear viscoelastic regime, where G' or G'' are dependent on %strain (Figures 4.35, 4.36 and 4.37). This can be explained by the elasticity of the ER fluid, which is dominated by the particle chain structures in an imposed electric field. The fibrillate structures of the suspended PBA-1 particles are spanned throughout electrodes by an applied electric field. Above a certain degree of deformation, the structure is broken down, and the elasticity of the ER Fluid abruptly decreases (Cho *et al.*, 1998). For the electric field strength of 2 kV/mm, G' is larger than G'' in both the linear and nonlinear viscoelastic regimes (Figure 4.34). This is because this suspension behaves as solid-like under this electric field strength even at very high deformation. So the response of the 10 wt% PBA-1 suspension at electric field strength of 2 kV/mm is superior than those of the polyaniline suspension. In addition, the range of a linear viscoelastic is broader than polyaniline suspension (Mata, 2000). On the other hand, G' at electric field strengths of 0.25, 0.02 and 0 kV/mm are smaller than G'' both in linear and nonlinear viscoelastic regimes (Figures 4.38, 4.39 and 4.40). Because this suspension behaves as fluid-like at these electric field strengths even at very low deformation.

4.3.2 Transient Response

Figure 4.41 shows G' and G'' responses to an electric step field of 2 kV/mm of 10 wt% PBA-1 suspension by the time sweep test at the frequency of 1 rad/s and 0.1 %strain. Under the electric step field application, the electric field of 2 kV/mm was repeatedly applied and released, the suspensions responded and equilibrated with the applied electric field within 30 s, which is faster than that of the polyaniline suspension (Mata, 2000). When the electric field was released, the G' and G'' of the sample recovered but did not completely recover to the original values possibly due to the strong

hydrogen bondings (H-bonding) between very small adjacent particles (Kroschwiz and Mary, 1995).

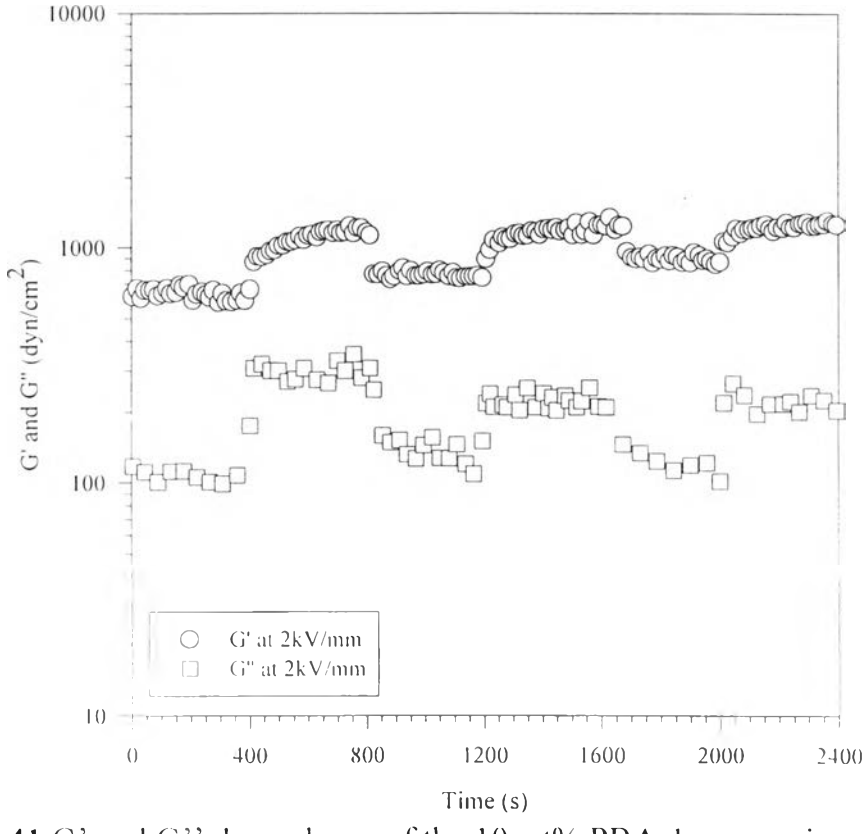

Figure 4.41 G' and G'' dependence of the 10 wt% PBA-1 suspension at the electric step field strength of 2 kV/mm and frequency of 1 rad/s

4.3.3 Effect of Frequency

4.3.3.1 *Linear viscoelastic regime*

The measurement was performed with the frequency sweep measurement. The frequency was varied from 0.05-100 rad/s. We chosed a strain in linear viscoelastic regime of a 0.1% strain for the electric field strengths of 2, 1 and 0.5 kV/mm, a 0.5 %strain for the electric field strength of 0.4 kV/mm, a 2 %strain for the electric field strength of 0.25 kV/mm, and a 10 %strain for the electric field strengths of 0.02 and 0 kV/mm. This experiment was carried out to investigate the rheological behaviors as functions of the frequency and electric field strength. This experiment cannot

be compared with polyaniline suspension due to the limitation of %strain in its linear viscoelastic regime.

Figures 4.42 and 4.43 show the result of a frequency sweep test of 10 wt% PBA-1 suspension at various electric field strengths in the linear viscoelastic regime. The storage modulus (G') and the loss modulus (G'') were measured as a function of frequency. At zero electric field, ER sample behaves like a viscous fluid in which the G'' is much higher than G' over the entire range of frequency. With an applied the electric field to the sample, the chain-like or fibrillated structure is formed in the suspension. The formation of the particle chains increases the resistance of fluid motion, which can be represented by the storage modulus (G'). G' increases with the electric field strength under linear viscoelastic conditions, i.e. they become more elastic. On comparing the magnitude of the storage and the loss modulus at the electric field strengths of 0.02 and 0.25 kV/mm, as represented by Figure 4.42 with Figure 4.43, G' are lower than G'' over the entire range of frequency. These may be due to the fact that the chains are not completely expanded across the gap but they form separated short chains or attach to only one electrode. The storage modulus of the electric field strengths of 0.4, 0.5, 1 and 2 kV/mm seems to depend weakly on frequency in the presence of the electric field but is strongly electric field dependent.

In Figure 4.43, under no electric field, G'' increases linearly with frequency with the scaling exponent equal to 1 due to the fluid-like behavior. In the presence of the electric field, G'' increases with increasing electric field strength because of the electric field strengthenes the electrostatic force at the contact area of the neighboring particles. If the electrostatic force between adjoining particles in a particle chain is increased, the strength of the chain can be enhanced, resulting in a greater ER effect (Yatsuzuka *et al.*, 1995). For the electric field strengths of 0.02 and 0.25 kV/mm, there are no plateau and the scaling exponent equal to 1, because the

very small number of chains are formed, or form only short separated chains, or attach to only one electrode. For electric field strengths of 0.4, 0.5, 1 and 2 kV/mm, the increase in G'' with the applied electric field at low frequency is more pronounced than that at high frequency. G'' shows a stronger frequency dependence at a lower electric field. It can be observed that G'' of 10 wt% PBA-1 suspension at these electric field strengths exhibit plateaus in the presence of the electric field due to the forming of the chain-like or fibrillate structure. The width of the plateau also depends on the electric field strength. The higher the electric field strength the broader the width of the plateau is observed. It can be concluded that the ER sample has a greater resistance to flow when the electric field strength is greater. However, at high frequency, G'' becomes similar to that without an electric field, ER effect tends to diminish. The presence of the electrostatic field does not affect the rheological property of the sample in high frequency regime because the structure distorts.

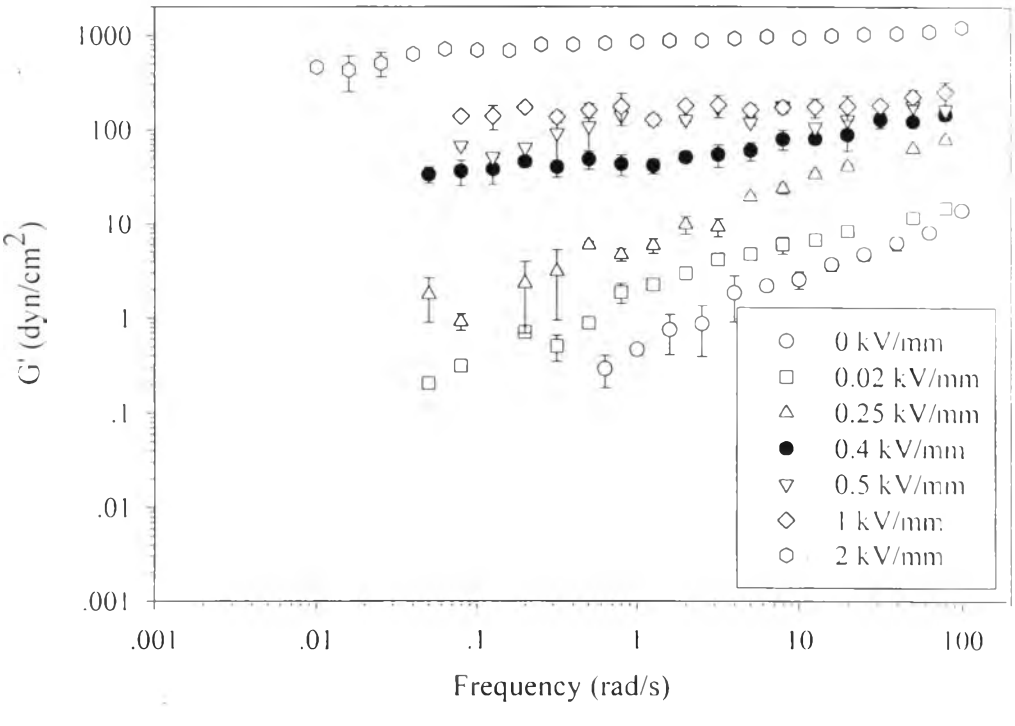

Figure 4.42 G' dependence on frequency of 10 wt% PBA-1 suspension at various electric field strengths in the linear viscoelastic regime.

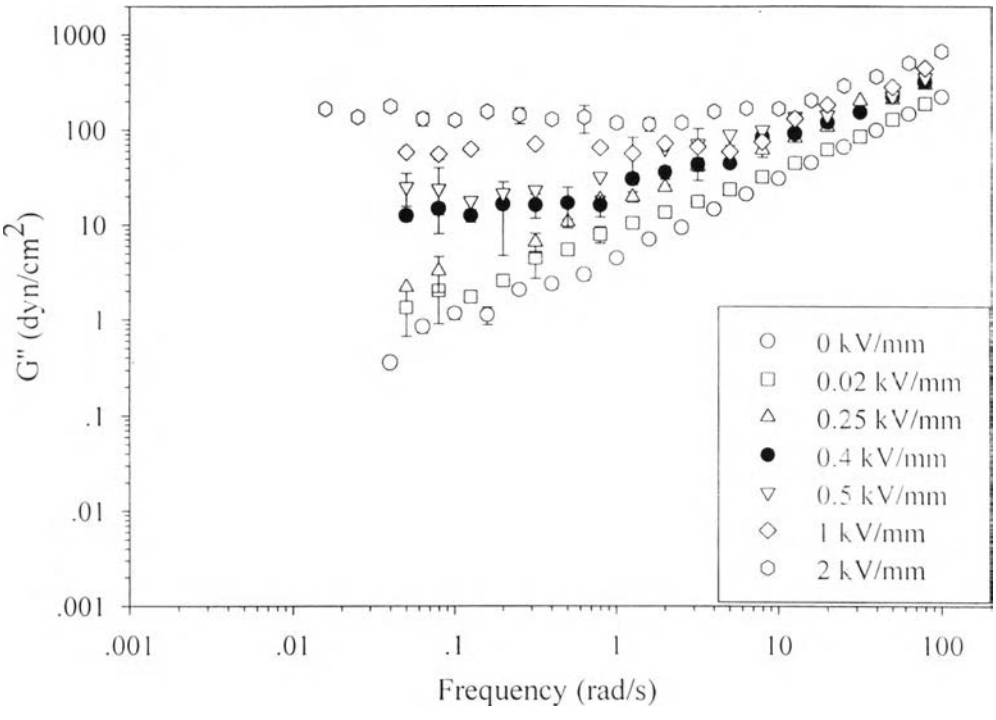

Figure 4.43 G'' dependence on frequency of 10 wt% PBA-1 suspension on various electric field strength in linear viscoelastic regime.

Upon increasing the electric field strength, it can be seen in Figure 4.44 that in the presence of 0.4 kV/mm electric field, G' is higher than that of G'' at low frequency (< 8). These field-induced structure are viscoelastic in that a predominantly elastic response is observed at low deformation, but at higher frequencies particle motion produces a more viscous response. At higher frequency, the viscous behavior is more dominant. When comparing between 0.4, 0.5 and 1 kV/mm electric field strengths (Figures 4.44, 4.45 and 4.46), the crossover points of G' and G'' are 8, 15 and 20 rad/s at electric field strengths 0.4, 0.5 and 1 kV/mm, respectively due to the stronger electrostatic force between the particles in the chains. For the electric field strength of 2 kV/mm (Figure 4.47), the storage modulus is higher than the loss modulus at all frequency. Because this suspension behaves as solid-like under this electric field strength even at very high deformation.

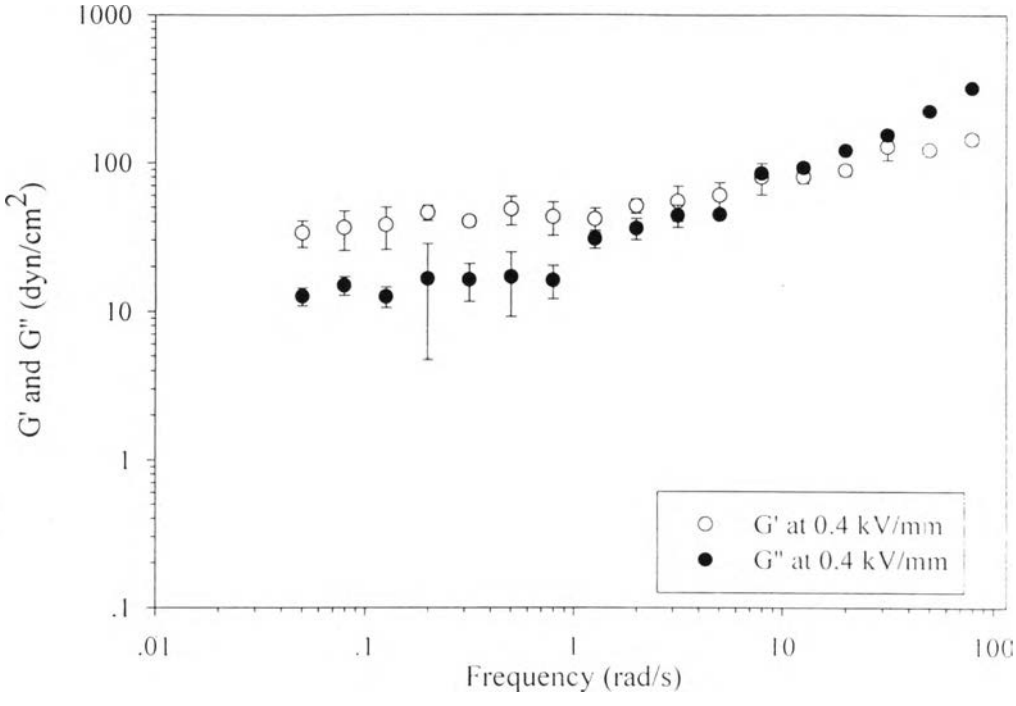

Figure 4.44 G' and G'' dependence on frequency of 10 wt% PBA-1 suspension in the linear viscoelastic regime at the electric field strengths of 0.4 kV/mm.

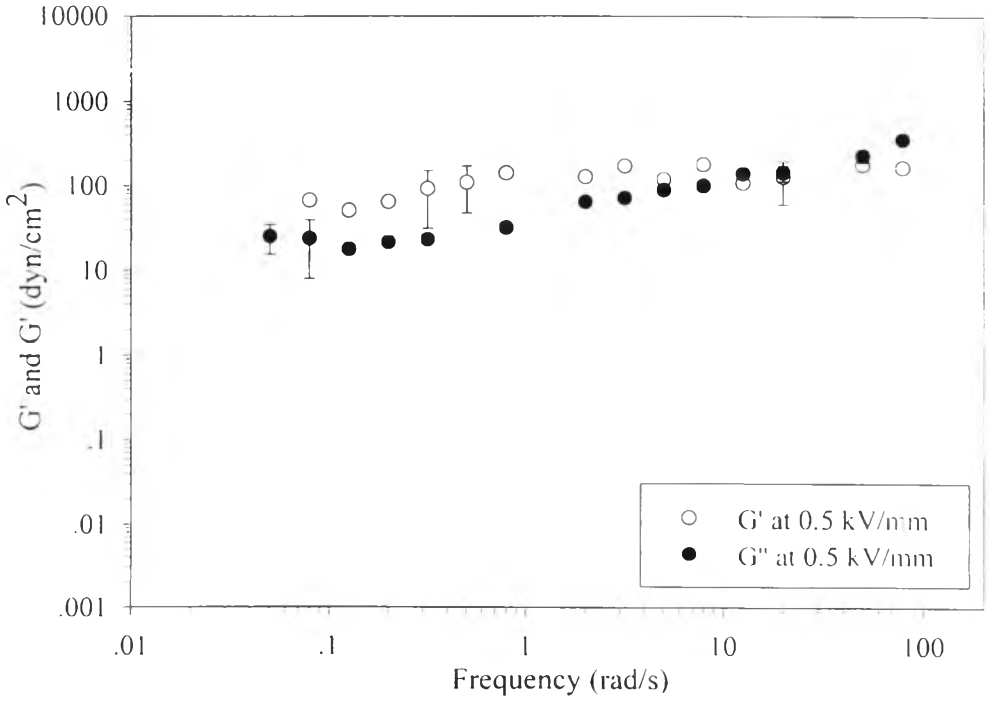

Figure 4.45 G' and G'' dependence on frequency of 10 wt% PBA-1 suspension in the linear viscoelastic regime at the electric field strengths of 0.5 kV/mm.

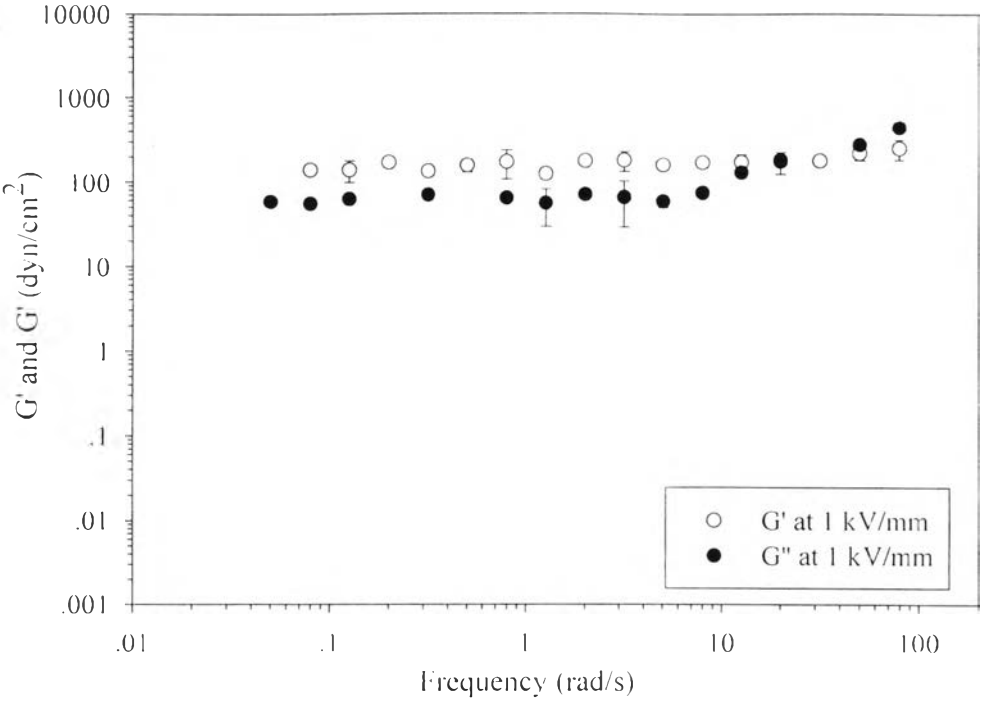

Figure 4.46 G' and G'' dependence on frequency of 10 wt% PBA-1 suspension in the linear viscoelastic regime at the electric field strengths of 1 kV/mm.

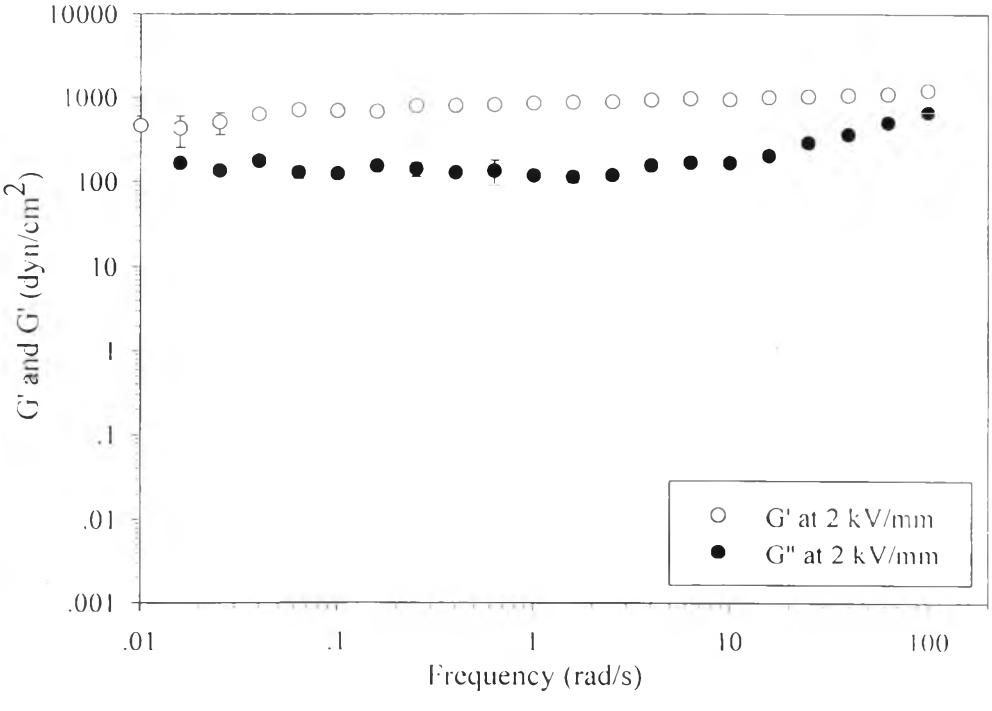

Figure 4.47 G' and G'' dependence on frequency of 10 wt% PBA-1 suspension in the linear viscoelastic regime at the electric field strengths of 2 kV/mm.

The tan δ as a function of frequency at the 0, 0.02, 0.25, 0.4, 0.5, 1 and 2 kV/mm electric field strengths for the 10 wt% PBA-1 suspension is shown in Figure 4.48. The tangent of the phase angle δ, tan δ, is the ratio of the out-of-phase to in-phase component: tan $\delta \equiv G''(\omega)/G'(\omega)$. For electric field strengths of 0, 0.02 and 0.25 kV/mm, tan δ is higher than 1 at all frequency due to fluid-like behavior even at low deformation. Beyond these electric field strengths, tan δ decreases with electric field strength. This ratio demonstrates that at electric field strengths of 0.4, 0.5, and 1 kV/mm at low frequencies the in-phase modulus (G') dominates. Whereas the electric field strengths of 2 kV/mm, tan δ is lower than 1 at all frequency due to solid-like behavior even at high deformation.

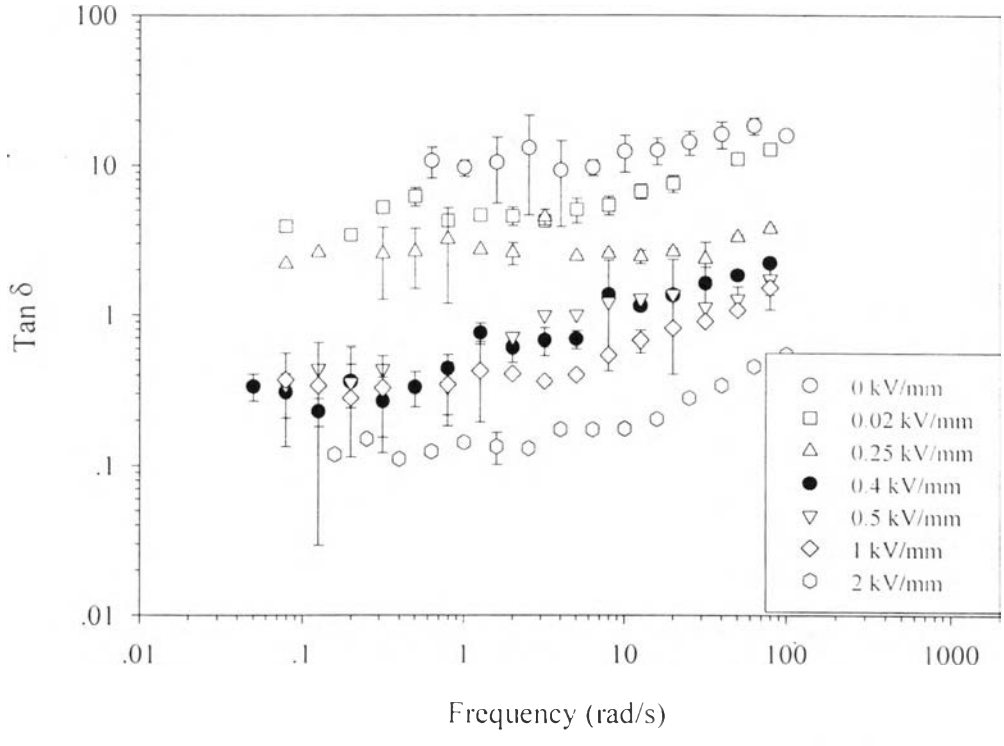

Figure 4.48 Tan δ dependence on frequency of 10 wt% PBA-1 suspension at various electric field strengths in the linear viscoelastic regime.

The characteristic values of the storage and loss modulus at frequency of 0.001 rad/s, $[G']_0$ and $[G'']_0$, at various electric field strengths in the linear viscoelastic regime is shown in Figure 4.49 (their raw data are tabulated in Appendix F). There are 2 regimes. At electric field strength below 0.25 kV/mm, Regime I, the suspension shows a fluid-like behavior because all $[G'']_0$ values are larger than $[G']_0$. Both values slightly increase with the electric field strengths due to the weak electrostatic force between the particles in the chains. The increase in $[G'']_0$ at low applied electric field is more pronounced than at high applied electric field. In Regime II, where the electric field strength is above 0.4 kV/mm, the suspension shows a solid-like behavior because all $[G']_0$ values are larger than $[G'']_0$. Both values rapidly increase with the electric field strengths due to the strong electrostatic force between

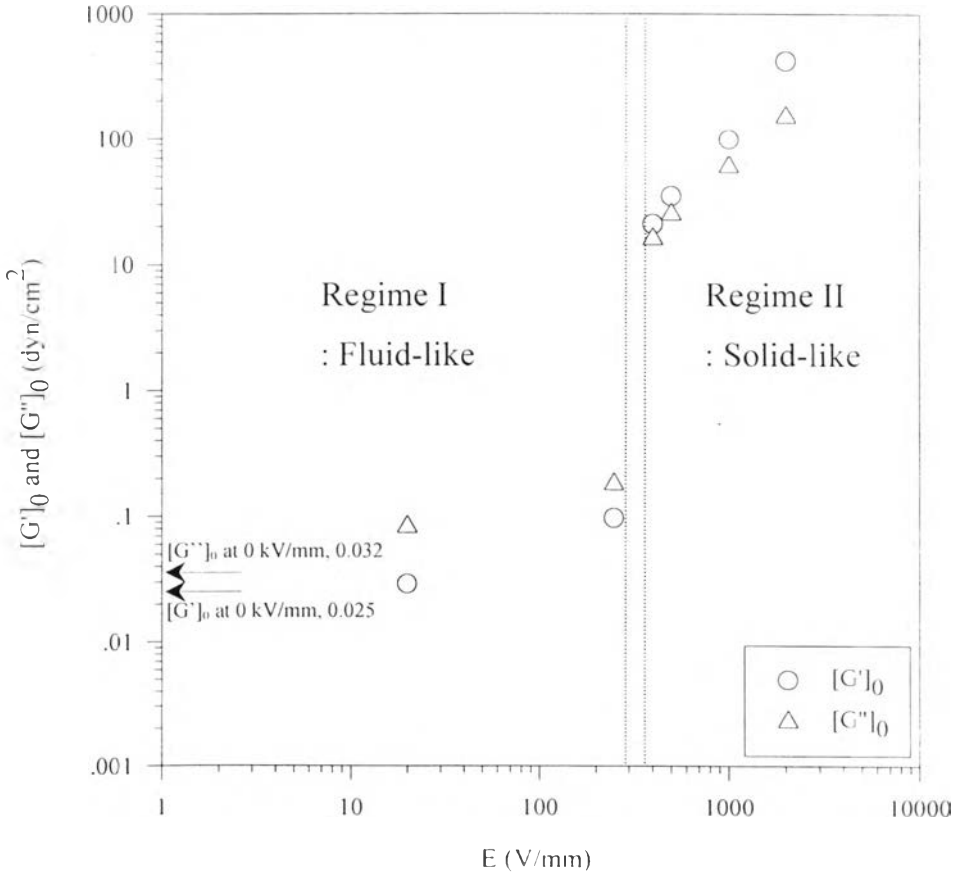

Figure 4.49 $[G']_0$ and $[G'']_0$ at various electric field strengths in the linear viscoelastic regime.

the particles in the chains. The increase in $[G']_0$ at high applied electric field is more pronounced than at low applied electric field. The very interesting part is the region between the electric field strengths of 0.25 and 0.4 kV/mm. There is a critical electric field strength for the transition from liquid to solid state.

4.3.3.2 *Nonlinear viscoelastic regime*

We studied the effect of the electric field strength in the nonlinear viscoelastic regime, which is useful for designing many devices, such as active engine mounts, sock absorber, clutches, brakes and robotic devices. Most of these devices operate in dynamic or transient modes where the fluid will be subjected to finite deformations (Parthasarathy and Klingenberg, 1999). The experiment was performed with the frequency sweep measurement in nonlinear viscoelastic regime at a constant %strain (600%) for all electric field strengths (0, 0.02, 0.25, 0.5, 1, 2 kV/mm). The frequency was varied from 0.05-100 rad/s. The rheological properties of this suspension were measured as a function of electric field strength. Many structuring fluids such as suspensions and polymer solution show nonlinear viscoelasticity under large deformation. A dominating viscous contribution to the total dynamic response, the elastic effect in electrified ER fluid can be negligible at large strains. So we will not mention about the storage modulus in the nonlinear viscoelastic region.

Figure 4.50 shows the result of frequency sweep measurements of 10 wt% PBA-1 suspension at various electric field strengths in the nonlinear viescoelastic regime. The loss modulus (G'') was measured as a function of frequency. Under the electric field strengths of 0, 0.02, 0.25 and 0.5 kV/mm, G'' increase with frequency with the scaling exponent equal to 1. For the electric field strengths of 1 and 2 kV/mm, the increase in G'' at low frequency is more pronounced than at high frequency. This can be explained by cluster statistics and micro-structural observations, showing that the response at large strain amplitudes and small frequencies is dominated by

rupture and reformation of chains. At large frequency, the suspension behavior is similar that of a purely viscous fluid. Fibrous structures observed at lower frequency are degraded into much smaller aggregates under large strain amplitude (Parthasarathy and Klingenberg, 1999). Further more, these G'' values are smaller than those of in linear viscoealstic regime for all electric field strengths due to the large deformation of the chain structures.

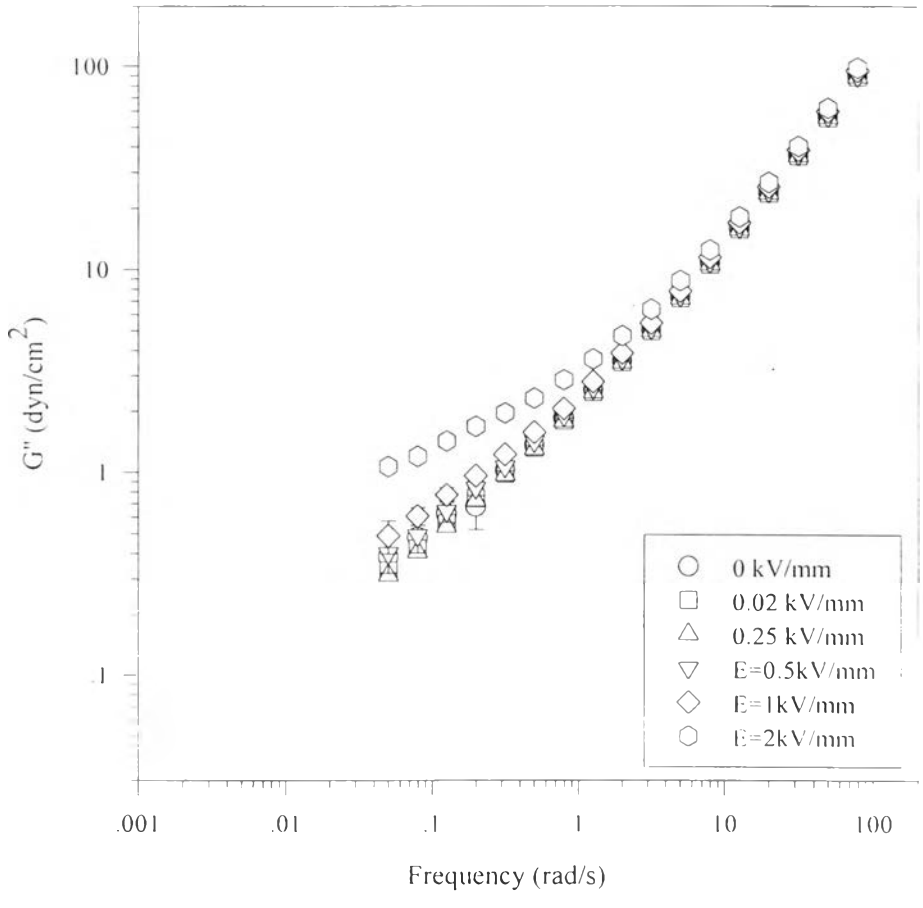

Figure 4.50 G'' dependence on frequency of 10 wt% PBA-1 suspension at various electric field strengths in the nonlinear viscoelastic regime.

The characteristic values of the loss modulus at frequency of 0.001 rad/s, $[G'']_0$, at various electric field strengths in the nonlinear viscoelastic regime is shown in Figure 4.51 (its raw data are tabulated in Appendix F). They can be classified to be 2 regimes. Both regimes show a fluid-like behavior because of the breakdown of internal fibrous structures under large deformation (Otsubo *et al.*, 1998). At electric field strength below 0.5 kV/mm, Regime I, exhibits plateau because the chains cannot be reformed at low frequency under large deformation. Whereas Regime II, where the electric field strength is above 0.5 kV/mm, the chains can be reformed at low frequency under large deformation. The higher the electric field strength the higher the reformation of chains is observed so the increase in $[G'']_0$ at high applied electric field is more pronounced than at low applied electric field.

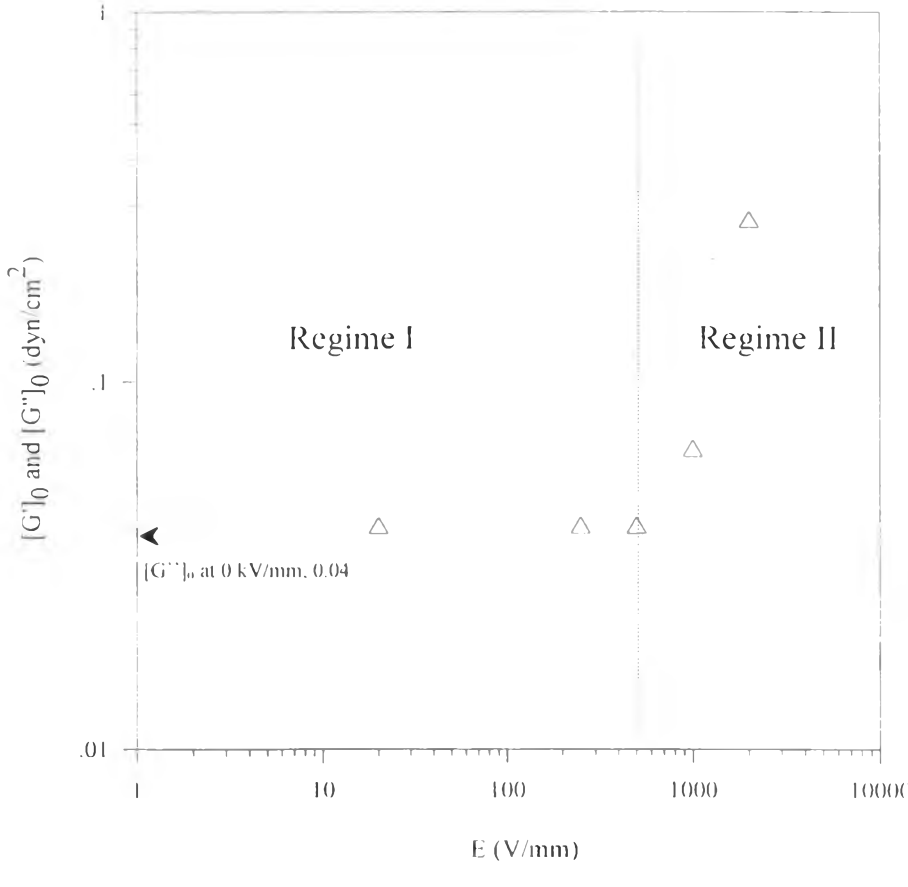

Figure 4.51 $[G'']_0$ at various electric field strengths in the nonlinear viscoelastic regime.